Pattern formation on a periodic rectangle and the Green's function Potential

Arvin Varizy, Hansol Park, and Theodore Kolokolnikov[1]

[1] *Department of Mathematics and Statistics, Dalhousie University Halifax, Nova Scotia, B3H3J5, Canada**

Many reaction-diffusion systems exhibit spot patterns. When the domain is a periodic rectangle, many such patterns can be constructed explicitly using regular integer lattices, and moreover numerical simulations show that they are prevalent even when starting with random initial conditions. For a wide class of RD systems which includes the Schnakenberg model, these equilibria are local minima of the a corresponding Green's function potential. We use integer lattice enumeration and Floquet theory to classify all stable such lattices on a square up to $N = 200$ spots. We then investigate stability boundaries and bifurcations as the aspect ratio of the rectangle is varied. For a rectangle with a small aspect ratio, we derive explicit thresholds for stability of a pattern consisting of two interlaced stripes. For certain aspect ratios and N, there exist a perfect hexagonal lattice without any defects. We determine stability boundaries of such lattices as the aspect ratio changes. We also explore bifurcations and transitions that result when the lattice is deformed beyond its stable regime. The results are illustrated and confirmed using the Schnakenberg reaction-diffusion system.

1. INTRODUCTION

Many reaction-diffusion systems exhibit spot patterns. In certain limits when spots become localized, their dynamics and equilibria locations can be be asymptotically described by a system of ODE's for spot centers. The resulting pattern arises as a stable equilibrium of this reduced ODE system. For a general bounded two-dimesional domain, these reduced equations are typically too complex to solve explicitly, except for some special situations such as a disk domain [1], or in the continuum limit of many spots [2]. In this paper we consider the case when the domain is a rectangle with periodic boundary conditions. Such domains are often used for numerical simulations due to simplicity of implementing the Laplace operator on a rectangle, going as far back as the original paper of Turing [3].

Spot locations for certain RD systems as well as many other problems have a unifying description in terms of Green's function energy. This potential arises in a variety of problems; see e.g. [4–7] and references therein. Let us highlight some of them.

Problem 1. Mean First Passage Time (MFPT) on a domain with small traps. [4, 6–10] Consider a brownian particle moving inside a rectangular domain

$$\Omega = \{(x, y) : 0 \le x \le L, 0 \le y \le H\},$$

subject to periodic motion, so that (x, y) is taken $\bmod (L, H)$. Suppose that the domain Ω contains N small traps, where each trap trap is a disk of radius ε centered at $x = \xi_k$, denoted by $B_\varepsilon(\xi_k)$. The particle is absorbed if it hits one of the traps. Let $u(x)$ be the expected time for the particle to be absorbed if it starts from location x. After some

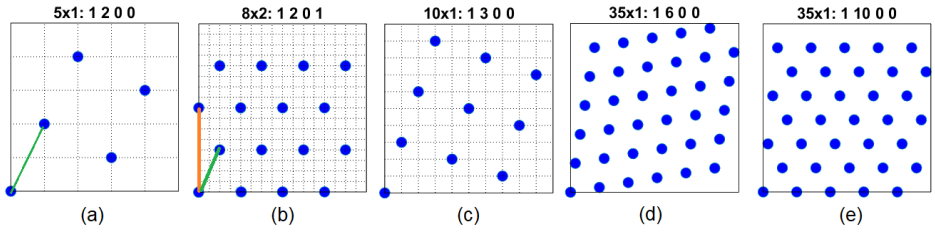

FIG. 1. Examples of integer lattices. (a) $N = 5$, generated by by a single vector $v_1 = (1, 2)$ (on a square of sides $N \times N$). (b) $N = 16$, generated by two vectors $v_1 = (2, 4)$ and $v_2 = (0, 8)$. (c-e) Some further examples, all generated by a single vector. Each title has the format $n_1 \times n_2 : a\ b\ c\ d$ as given by (1.7).

* tkolokol@gmail.com

rescaling, u satisfies

$$\begin{cases} \Delta u + 1 = 0 \text{ inside } \Omega \backslash \bigcup\limits_j B_\varepsilon(\xi_j) \\ u = 0 \text{ on } \bigcup_j \partial B_\varepsilon(\xi_j). \\ u \text{ is periodic on } \partial\Omega\text{: } u(0,x_2) = u(L_1,x_2) \text{ and } u(x_1,0) = u(x_1,L_2) \end{cases} \tag{1.1}$$

The Mean First Passage Time (MFPT) is defined to be the *average* of $u\,(x)$:

$$MFPT := \frac{1}{LH} \int\limits_{\Omega \backslash \bigcup B_\varepsilon(\xi_j)} u(x)dx.$$

A natural question is: *how should the traps be arranged to capture the brownian particle as fast as possible, that is, to minimize MFPT?*

Problem 2. Fundamental eigenvalue of the Laplacian. This is the eigenvalue problem

$$\begin{cases} \Delta u + \lambda u = 0 \text{ inside } \Omega \backslash \bigcup\limits_j B_\varepsilon(\xi_j) \\ u = 0 \text{ on } \bigcup_j \partial B_\varepsilon(\xi_j). \\ u \text{ is periodic on } \partial\Omega \end{cases} \tag{1.2}$$

where notation is the same as in MFPT problem. The goal is to arrange traps to minimize the principal eigenvalue λ.

Problem 3. Spike equilibria and stability for the Schnakenberg and other reaction-diffusion systems. Here, we are interested in spike patterns consisting of N spikes and their stability for the Schnakenberg model on a periodic domain. Using the scaling from [1], the model is

$$u_t = \varepsilon^2 \Delta u - u + u^2 v, \qquad 0 = \Delta v + A - u^2 v \frac{1}{\varepsilon^2} \frac{1}{\log \varepsilon^{-1}}, \tag{1.3}$$

where $\varepsilon \ll 1$ is a small parameter and A is called the "feed rate". The system is scaled in this particular way to assure that the height of the spots is of $O(1)$ in the inner region as $\varepsilon \to 0$.

All three problems above (and many others, see e.g. [7]) have, at their core, the following optimization problem. Define the Modified Green's function to satisfy

$$\Delta G - \frac{1}{|\Omega|} + \delta\,(x) = 0; \quad \int\limits_\Omega G = 0; \quad G \text{ is periodic on } \partial\Omega. \tag{1.4}$$

Define the **Green's function interaction potential (or energy)** to be

$$E\,(\xi_1, \ldots \xi_N) := \sum_{k=1}^{N} \sum_{j=k+1}^{N} G(\xi_k - \xi_j). \tag{1.5}$$

It was shown in [7] that all three problems are related to E. The optimal trap locations for MFPT problem (1.1) correspond to the (global) minimizer of E. Same applies for the eigenvalue problem (1.2). Finally, equilibrium spike locations for the Schnakenberg model correspond to a critical point E; stable equilibria correspond to its local minima. In fact, consider the gradient flow corresponding to the functional (1.5),

$$\frac{d}{dt}\xi_k = -\sum_{j \neq k} \nabla G(\xi_k - \xi_j) \tag{1.6}$$

As is well established, spike dynamics for many reaction-diffusion systems such as for the Schnakenberg model [11, 12], or certain limits of Gierer-Meinhardt model [11, 13, 14], to leading order, follow the same gradient flow, up to a temporal rescaling.

In this work we study a family of highly symmetric equilibria of (1.6), as well as their associated stability. The family in question are *periodic lattice patterns*. Given $N = n_1 n_2$, an integer lattice of N is a subset of $\mathbb{Z}_N \times \mathbb{Z}_N$ constructed as follows, from two basis vectors:

$$\tilde{L} = \{(a,b)\, n_2 j_1 + (c,d) n_1 j_2 \pmod N : j_1 \in Z_{n_1}, \quad j_2 \in Z_{n_2}\}; \quad (a,b) \in \mathbb{Z}^2_{n_1}, \quad (c,d) \in \mathbb{Z}^2_{n_2}, \quad n_1 n_2 = N \tag{1.7}$$

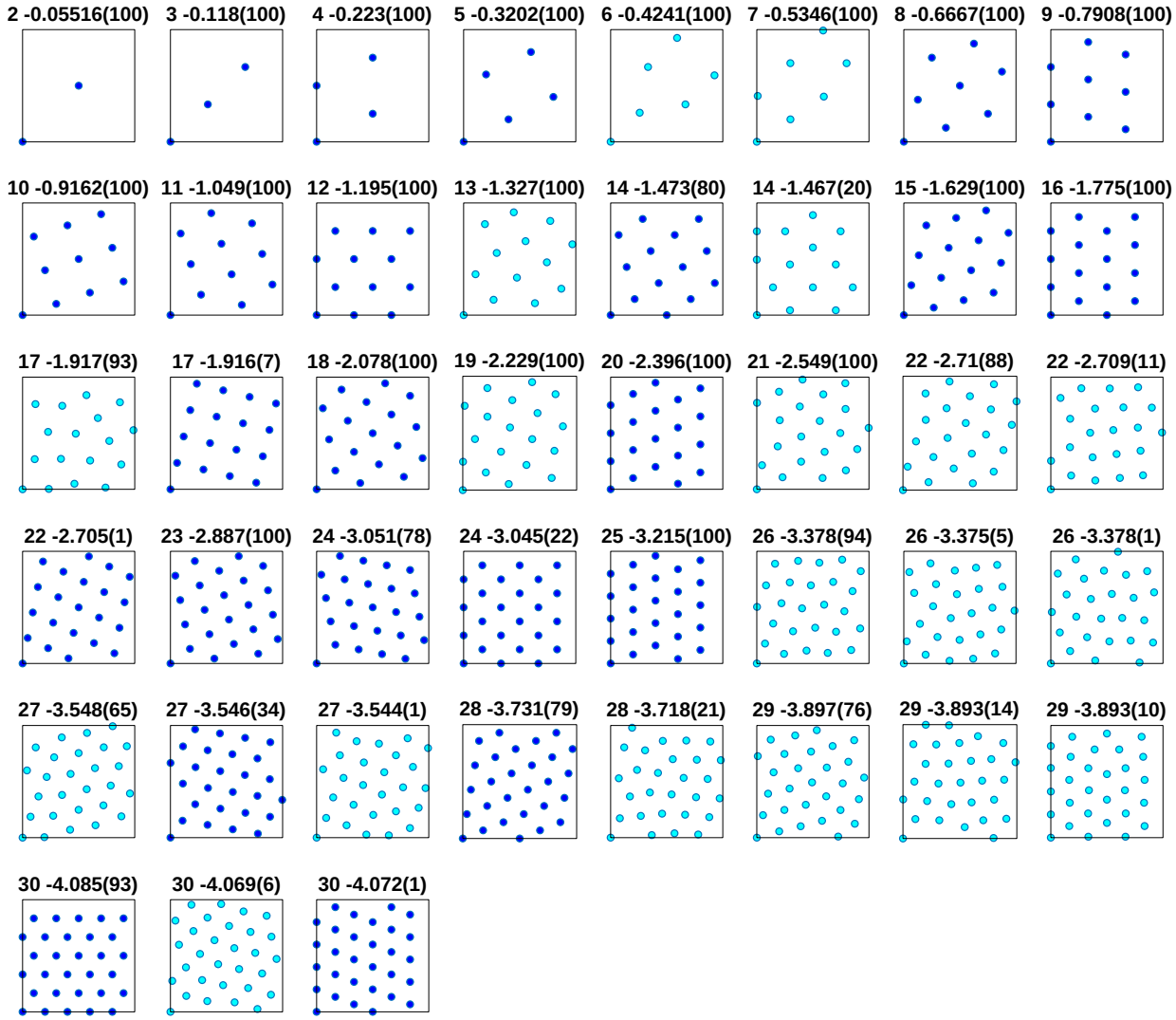

FIG. 2. Stable equilibria of the gradient flow (1.6) for $N = 1 \dots 30$. For each N, 100 simulations of (1.6) were computed, starting with random initial conditions. The simulation was ran until the it converged to an equilibrium state. Each subfigure has caption $N, E(\#)$ where N is the number of particles, E is the energy (1.5) at the equilibrium, and $\#$ is the number of times (out of a total 100) the simulation converged to it. Blue equilibria correspond to lattice equilibria whereas cyan correspond to non-lattice ("irregular") equilibria.

where arithmetic is taken mod N. Not all choices of a, b, c, d generate distinct N points, and many different choices can generate the same set. We call this set a lattice of size N if the size of $\tilde{L}$ is exactly N.

From an integer lattice of N points, we obtain a *regular lattice* inside the rectangle Ω by simply scaling the sides appropriately:

$$\begin{aligned} L &= \left\{ \left(x\frac{L}{N}, y\frac{H}{N} \right) : (x, y) \in \tilde{L} \right\} \\ &= \{ v_1 j_1 + v_2 j_2 \ (\mathrm{mod}\, \Omega) : (j_1, j_2) \in \mathbb{Z}_{n_1} \times \mathbb{Z}_{n_2} \}, \quad v_1 = (aL, bH)\,\frac{1}{n_1}, \quad v_2 = (cL, dH)\,\frac{1}{n_2} \end{aligned} \tag{1.8}$$

Figure 1 illustrates some examples of such lattices. A special case is when $n_2 = 1$, in which case this lattice is generated by a single vector ($v_2 = 0$).

A key property of any lattice is that if any two points $p, q \in L$, then the reflection of q with respect to p, namely,

$q^R = p - (q-p) \pmod{\Omega}$ is also in L. This, together with the fact that $G(z) = G(-z)$, implies that any lattice is automatically an equilibrium of the gradient flow (1.6).

The number of integer lattices of size N has been enumerated in [15]; it is shown there that up to rotations and reflections, the number of such lattices with N points is given by the generating function

$$\sum_{m=1}^{\infty} \left[\frac{1}{(1-t^m)(1-t^{4m})} - 1 \right] \tag{1.9}$$

(sequence https://oeis.org/A145393 in OEIS). For example, up to rotations and reflections, there are exactly 21 distinct such lattices when $N = 24$; these are shown in Appendix B. However most of these lattices are saddle points, not local minima of the energy (1.5). Here, we address the question of *stability* of these lattices with respect to the gradient flow (1.6). Local minima correspond to the stable equilibria of the gradient flow (1.6).

Figure 2 show stable equilibria attained by the gradient flow (1.6) starting with random initial conditions and N particles, $N = 2 \dots 30$. For each N we ran 100 simulations; the number of simulations converging to the particular equilibria is shown in the figure. Blue equilibria correspond to lattice equilibria whereas cyan correspond to non-lattice ("irregular") equilibria. For example when $N = 14$, 80% of simulations converged to a lattice equilibrium and 20% converged to an irregular equilbrium. Overall, lattice equilibria feature prominently; for many N (e.g. $N = 30$), lattice equilibria are the presumed global minima.

To determine stability requires to compute $2N$ eigenvalues of the linearization of the flow (1.6) around its equilibrium. In Section 2 we use Floquet-type theory to decompose this problem into N 2x2 matrices. We use this decomposition, in conjunction with lattice enumeration, to find all of the stable lattices on a square up to $N = 200$. These results are shown in Appnendix B.

Proposition 1.1. *A rectangular $n_1 \times n_2$ lattice generated by vectors $v_1 = (1,0)\frac{L}{n_1}$ and $v_2 = (0,1)\frac{H}{n_2}$ is always unstable for any n_1, n_2 and any L, H.*

The instabilities of a rectangular lattice (including a special case of a single row of particles) are illustrated in Figure 1(a-c).

The aspect ratio $\rho = L/H$ of the domain also has a dramatic effect on lattice stability, and different lattices "win" the stability race as the aspect ratio is changed; see Figure 1d-f) as well as Appendix B. Washen aspect ratio is sufficiently small, a lattice that consists of two rows of interlaced (phase-shifted) particles is stable, but is destabilized as the ratio is increased. This is illustrated in Figure 1(d-f). In section §3 we analyse stability of such a configuration in the limit of large N. We show the following result.

Proposition 1.2. *Consider a lattice of N spots generated by a single vector $v = \left(\frac{1}{2}L, \frac{1}{N}H\right)$: $\xi_j = \left(\frac{1}{2}L, \frac{1}{N}H\right) j \pmod{\Omega}$, $j = 0 \dots N-1$, with N even. This lattice consists of two interlaced vertical stripes as illustrated in figure 1(c). Such a lattice is stable provided that $\frac{H}{NL} \geq a_0$, where the constant $a_0 \approx 0.48209$ is the root of*

$$\sum j^2 \frac{(-1)^j e^{-\pi a_0 j}}{\left(1-(-1)^j e^{-\pi a_0 j}\right)^2} = 0. \tag{1.10}$$

It is unstable otherwise.

An important special case is a hexagonal lattice. Such a lattice can be obtained as follows. Let $n_1 = n$, $n_2 = 2n$, and consider a lattice of $N = n_1 n_2 = 2n^2$ particles generated by vectors

$$v_1 = \frac{1}{n}(L, 0); \quad v_2 = \frac{1}{2n}(L, H) \tag{1.11}$$

as illustrated on Figure 4. When the side ratio $L/H = \sqrt{3}$ (or $1/\sqrt{3}$), the corresponding lattice forms a perfect hexagonal pattern; this corresponds to the angle $\angle v_1 v_2 = 30^\circ$ (or 60°). We have the following result.

Proposition 1.3. *Consider a lattice generated by vectors (1.11) with $N = 2n^2$ points (refer to Figure 4). In the limit $n \to \infty$, this lattice is stable when H/L or $L/H \in (a_0, a_1) \approx (0.48209, 0.7678)$ (angle $\angle v_1 v_2$ between 25.73 and 37.52 degrees, or between 54.48 and 64.26 degrees). The threshold a_0 is given by (1.10) whereas the threshold $a_1 \approx 0.7678$ is a root of equations (4.23, 4.24, 4.27).*

Proposition 1.3 is illustrated in Figure 6 ($n = 4, N = 32$). Good agreement is observed, even for a relatively small value of $n = 2$.

We now summirize the rest of the paper. In §2 we show how to decompose the $2N \times 2N$ eigenspace of lattice stability of a lattice into N 2x2 matrices. In §§3-4 we use the decomposition formulas in conjunction with Fourier series solution of the Green's function and various asymptotic techniques to derive Propositions 1.1, 1.2, 1.3.

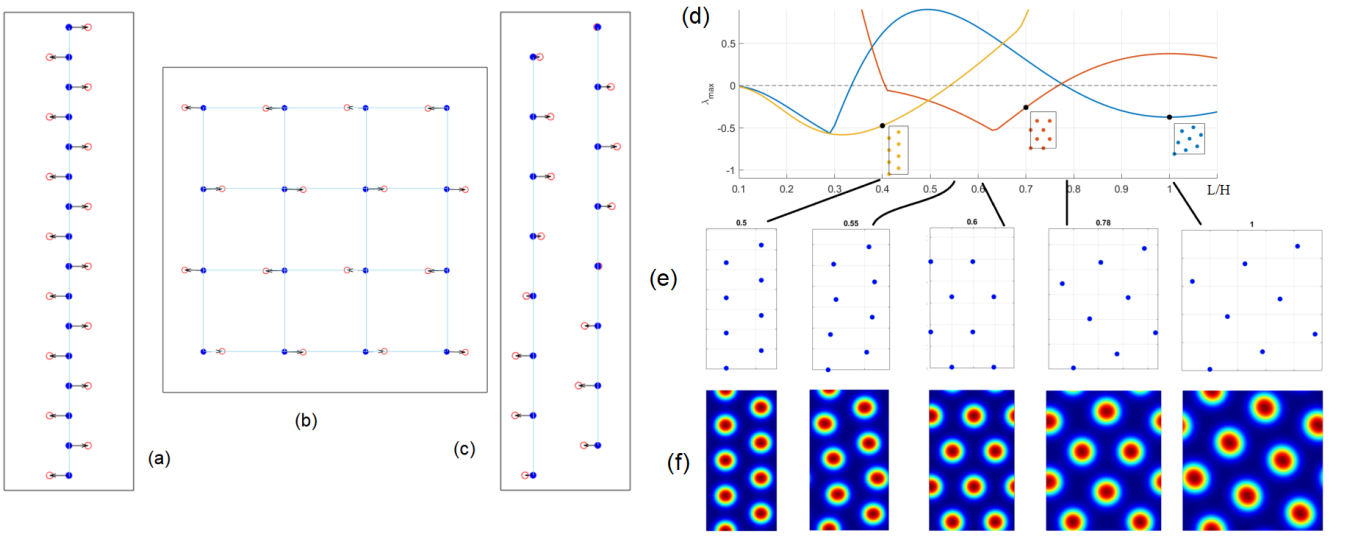

FIG. 3. (a-b): a rectangular lattice is always unstable (Proposition 1.1); the fastest destabilizing mode is shown. (c): Stability curve for different lattices as a function of rectangle aspect ratio L/H. The plot shows $\lambda_{\max}$, the biggest eigenvalue of the steady state corresponding to the gradient flow (1.6). The lattice is stable when $\lambda_{\max} < 0$. Inserts show different stable lattices for different aspect ratios. For sufficiently small aspect ratio, a two-stripe equilibrium becomes stable; see Proposition 1.2. (d): Equilibrium configurations obtained by solving the gradient flow (1.6) for aspect ratio L/H as indicated. For leftmost frame, random initial conditions were used. For subsequent frames, initial conditions of the previous frame were used, with small perturbations. First, third, and fifth frames are exact lattice patterns. Second and fourth are transitionary patterns. BOTTOM ROW: Full simulations of the Schnakenberg model (1.3) with aspect ratio as given. Other parameters were taken to be: $A = 26, \varepsilon = 0.05$, and with $LH = 4$. For leftmost frame, initial conditions consisting of 8 spots were used. Subsequent framems were initialized using the steady state of the preceeding frame.

2. STABILITY DECOMPOSITION FOR LATTICES

We now study stability of lattice equilibria with respect to the gradient flow (1.6). Although there are a total of $2N$ eigenvalues, due to the periodic nature of the lattice, the problem decomposes into N 2x2 subspaces, each represented by a 2x2 matrix, which we now derive.

For convenience of notation, write the lattice points using a double index $j = (j_1, j_2)^T$ in compact form as

$$\xi_j = \xi_{(j_1,j_2)} = vj = v_1 j_1 + v_2 j_2 \pmod{\Omega}. \tag{2.12}$$

Here, v is the 2x2 matrix $(v_1|v_2)$ and j_1 is taken mod n_1 and j_2 is taken mod n_2. We then write the gradient flow (1.6) as

$$x_k' = \sum_{j \neq k} G_1(x_j - x_k, y_j - y_k)$$
$$y_k' = \sum_{j \neq k} G_2(x_j - x_k, y_j - y_k).$$

Here, the indices represent vectors $k = (k_1, k_2)^T$ and $j = (j_1, j_2)^T \in Z_{n_1 \times n_2}$, and $\sum$ is the double sum having $n_1 n_2 - 1$ terms; and we denoted $G_1(x, y), G_2(x, y)) = \nabla G(x, y)$.

We linearize around the steady state equilibrium as follows. Let Linearize around it as:

$$x_k(t) = vk + e^{\lambda t}\phi_k, \quad y_k(t) = vk + e^{\lambda t}\psi_k,$$

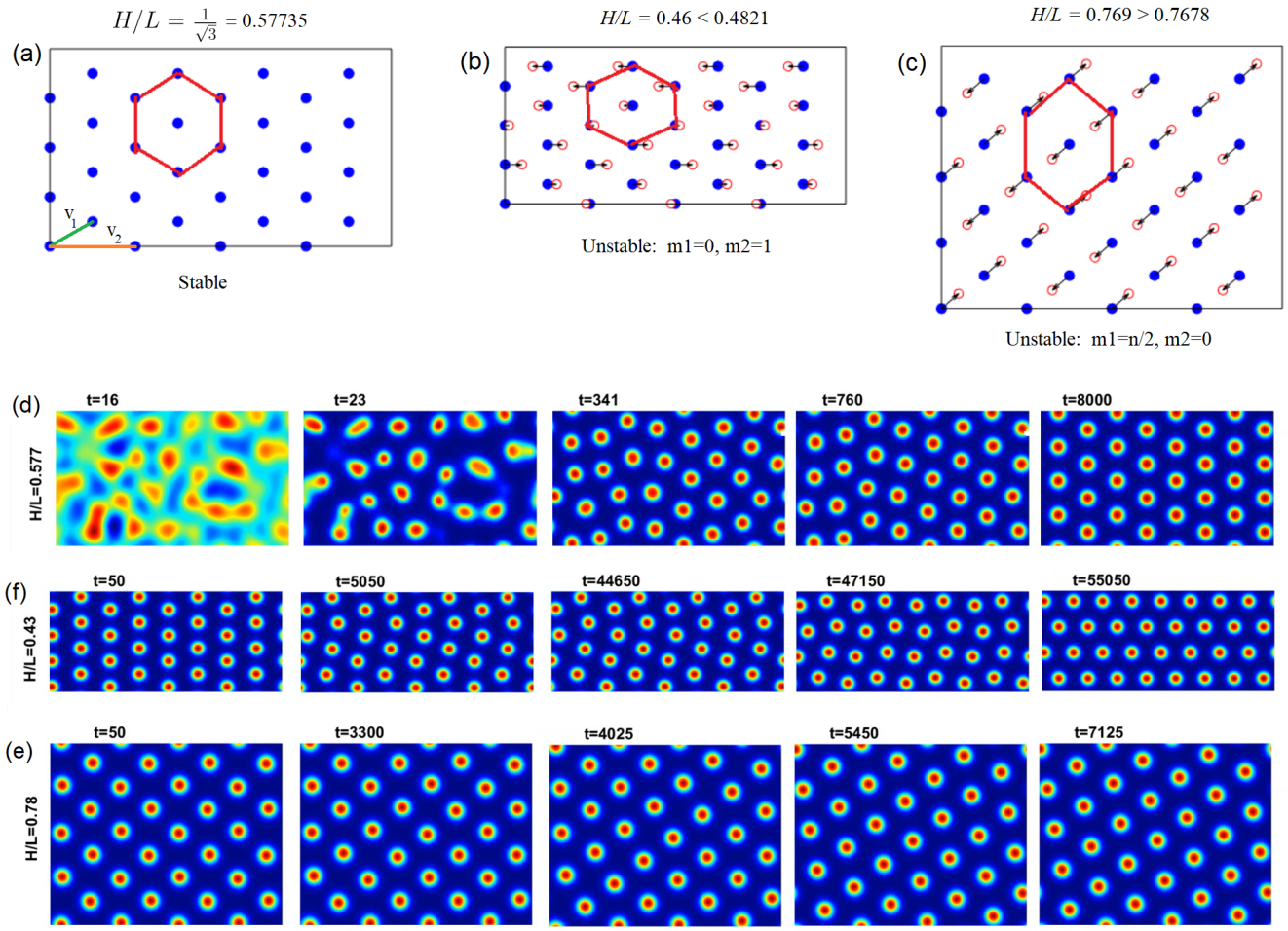

FIG. 4. (a) A perfect hexagonal lattice without any defects spanned by vectors (1.11) with $n = 4$, $N = 32$, with $H/L = 3^{-1/2}$. It is stable. (b) When H/L decreases below 0.4821, an instability corresponding to the mode $m_1 = 0, m_2 = 1$ emerges. The corresponding (destabilizing) eigenvector is shown. (c) When the the H/L increases above 0.7678, an instability corresponding to the mode $m_1 = n/2$, $m_2 = 0$ emerges. The corresponding eigenvector is shown. (d) Full numerical simulation of the Schnakenberg model starting with random initial conditions. Parameters are $\varepsilon = 0.024, D = 1, A = 123$, $L = 2.31$ and $H = L/\sqrt{3}$. Turing instabiliy leads to formation of 32 spots which then rearrange themselves into a perfect hexagonal lattice. (e) Same parameters as in (d) except H/L as indicated. Initial conditions are taken to be the final state in (d). The instability shown in figure (b) leads to a grid deformation into a wavy pattern. The resulting wavy state itself is borderline unstable eventually leading to another regular lattice equilibrium. (f) Here H is increased to $0.78L$. Initial conditions are taken to be the final state in (d). Instability A transition to a different regular lattice is observed. See also [16] for movies of the simulations.

to obtain the eigenvalue problem

$$\lambda\phi_k = \sum_{j\neq k} G_{11}(v\,(j-k))\,(\phi_j - \phi_k) + G_{12}(v\,(j-k))\,(\psi_j - \psi_k)$$
$$\lambda\psi_k = \sum_{j\neq k} G_{21}(v\,(j-k))\,(\phi_j - \phi_k) + G_{22}(v\,(j-k))\,(\psi_j - \psi_k)$$

The eigenspace then decomposes as follows:

$$\phi_k = \phi \exp\left(2\pi i\left(\frac{m_1}{n_1}k_1 + \frac{m_2}{n_2}k_2\right)\right), \quad \psi_k = \psi \exp\left(2\pi i\left(\frac{m_1}{n_1}k_1 + \frac{m_2}{n_2}k_2\right)\right) \tag{2.13}$$

Here, $m = (m_1, m_2) \in \mathbb{Z}_{n_1\times n_2}$ are a pair of the so-called Floquet multipiers or modes. By letting $j = k + l$ and using

periodicity, after some simplification we obtain a 2x2 eigenvalue problem

$$\lambda_{(m_1,m_2)} \begin{pmatrix} \phi \\ \psi \end{pmatrix} = M \begin{pmatrix} \phi \\ \psi \end{pmatrix}, \quad \text{where} \quad M_{a,b} = \sum_{l \in \mathbb{Z}_{n_1 \times n_2} \setminus (0,0)} G_{ab}(vl) \left(\exp\left(2\pi i \left(\frac{m_1}{n_1} l_1 + \frac{m_2}{n_2} l_2 \right) \right) - 1 \right). \tag{2.14}$$

Equations (2.14) yield the formula for the eigenvalues as a function of the modes m_1, m_2. There is a pair of zero eigenvalues corresponding to $(m_1, m_2) = (0, 0)$. These two eigenvalues correspond to translational invariance of the problem. Asides from this zero mode, we therefore define

$$\lambda_{\max} := \max_{(m_1,m_2) \neq 0} \lambda_{m_1,m_2}. \tag{2.15}$$

The lattice configuration is *stable* if and only if $\lambda_{\max} \leq 0$. Appendix B showcases all the possible lattices, including those that are stable and those that are not.

The entry M_{22} can be written in terms of M_{11} as follows. Note that $G_{yy} = -G_{xx} + \frac{1}{LH}$. It then follows from (2.14) that for any $(m_1, m_2) \neq (0, 0)$,

$$M_{22} = -\frac{N}{LH} - M_{11}. \tag{2.16}$$

3. STRIPES AND RECTANGLULAR LATTICES.

In this section we derive Propositions 1.1 and 1.2.

Rectanglar lattice. We begin derivation of Proposition 1.1. A rectangular lattice with $N = n_1 n_2$ points has the form

$$(x_j, y_j) = \left(\frac{1}{n_1} j_1 L, \frac{1}{n_2} j_2 H \right), \quad j = (j_1, j_2) \in \mathbb{Z}_{n_1} \times \mathbb{Z}_{n2}.$$

To show its instability, we use the decomposition of eigenspace into 2x2 matrices M (2.14). We start with M_{11}. Using the Fourier expansion (A.4) for G we have,

$$G_{xx} = -\frac{2\pi}{L^2} \sum_{m=1}^{\infty} m \cos\left(2\pi m \frac{x}{L} \right) \frac{\cosh\left((y - H/2) \frac{2\pi}{L} m \right)}{\sinh\left(\frac{2\pi}{L} m H/2 \right)}. \tag{3.17}$$

Consider the mode $m_1 = 0,\ m_2 = n_2/2$ (the unstable mode shown in Figure 1(b)). Then we obtain:

$$M_{11}(m) = -\frac{2\pi}{L^2} \sum_{j_1=0}^{n_1-1} \sum_{j_2=1}^{n_2-1} \sum_{q=1}^{\infty} q \cos\left(2\pi q \frac{1}{n_1} j_1 \right) \frac{\cosh\left(\left(\frac{1}{n_2} j_2 H - H/2 \right) \frac{2\pi}{L} q \right)}{\sinh\left(\frac{2\pi}{L} q H/2 \right)} \left(\exp\{\pi i j_2\} - 1 \right)$$

Note that

$$\sum_{j_1=0}^{n_1-1} \cos\left(2\pi q \frac{x_j}{L} \right) = \begin{cases} 0, & n | q \\ n, & n \not| q \end{cases}.$$

Setting $q = Q n_1$ we obtain

$$M_{11}(m) = -\frac{2\pi}{L^2} n_1^2 \sum_{j_2=1}^{n_2-1} \sum_{Q=1}^{\infty} Q \frac{\cosh\left(\left(\frac{1}{n_2} j_2 H - H/2 \right) \frac{2\pi}{L} Q n_1 \right)}{\sinh\left(\frac{2\pi}{L} q H/2 \right)} \left(\exp\{\pi i j_2\} - 1 \right)$$

Since $(\exp\{\pi i j_2\} - 1) \leq 0$, it follows that $M_{11} > 0$. By symmetry (rotating the rectangle 90 degrees), we similarly obtain $M_{22} > 0$. Moreover it is easy to check that $M_{12} = M_{21} = 0$. It follows that both eigenvalues of M are positive for this mode. This proves the instability of a rectangular lattice.

Two stripes. We now derive the threshold in Proposition 1.2. The pattern consists of two phase-shifted stripes and N even, as shown in Figure 1(c). It is generated by a single vector $v = \left(\frac{1}{2} L, \frac{1}{N} H \right)$. (i.e. $N = n_1 n_2$ with $n_1 = N, n_2 = 1$). Numerics indicate that for a sufficiently tall rectangle, such a configuration is stable. As the aspect ratio is increased, the mode that becomes unstable first in (2.14) corresponds to $m = m_1 = 1$, as illustrated in Figure

1(e). To determine the instability boundary, we must compute the associated matrix M in (2.14). We begin by computing the entry M_{11}. Let $n = N/2$. Split M_{11} into two parts: $M_{11} = I_1 + I_2$ where I_1 is the sum over the left n points ($x_j = 0, \quad y_j = jH/n, \quad j = 1 \dots n$) and I_2 over the right ($x_j = L/2, \quad y_j = (j+1/2)\,H/n, \quad j = 1 \dots n$). We obtain

$$I_1 = -\frac{2\pi}{L^2} \sum_{j=1}^{n} \sum_{m=1}^{\infty} m \frac{\cosh\left((j/n - 1/2)\,\frac{2\pi}{L} Hm\right)}{\sinh\left(\frac{2\pi}{L} mH/2\right)} \left(\exp\left(2\pi ij/n\right) - 1\right),$$

$$I_2 = -\frac{2\pi}{L^2} \sum_{j=0}^{n} \sum_{m=1}^{\infty} (-1)^m\, m \frac{\cosh\left(((j+1/2)/n - 1/2)\,\frac{2\pi}{L} Hm\right)}{\sinh\left(\frac{2\pi}{L} mH/2\right)} \left(\exp\left(2\pi i\,(j+1/2)/n\right) - 1\right).$$

We start with I_1. Interchange the summation and write I_1 as $I_1 = -\frac{2\pi}{L^2} \sum_{m=1}^{\infty} m J_1(m)$ where

$$J_1 = \sum_{j=1}^{n} \frac{\cosh\left((j/n - 1/2)\,\frac{2\pi}{L} Hm\right)}{\sinh\left(\frac{2\pi}{L} mH/2\right)} \left(\exp\left(2\pi ij/n\right) - 1\right).$$

Define $x = \frac{H2\pi}{Ln}$ and assume that $n \gg 1$, $H = O(n)$, so that $x = O(1)$ (this is the critical scaling for the boundary between stability and instability). In this case the dominant contribution to J_1 comes from j near 1 and n; moreover J_1 is purely real and is symmetric with respect to $j = n/2$. We then estimate

$$\frac{\cosh\left((j/n - 1/2)\,\frac{2\pi}{L} Hm\right)}{\sinh\left(\frac{2\pi}{L} mH/2\right)} \sim \exp(-2xmj)$$

and

$$\begin{aligned} J_1 &\sim 2 \sum_{j=1}^{\infty} \left\{\exp(-2xmj)\right\} \left(\cos\left(2\pi j/n\right) - 1\right) \\ &\sim -\left(2\pi/n\right)^2 \sum_{j=1}^{\infty} \exp(-2xmj) j^2 \end{aligned}$$

so that

$$I_1 \sim \frac{2\pi^3}{L^2 n^2} \sum_{m=1}^{\infty} \sum_{j=1}^{\infty} m \exp(-2xmj) \left(2j\right)^2$$

An analogous computation yields

$$I_2 \sim \frac{2\pi^3}{L^2 n^2} \sum_{m=0}^{\infty} \sum_{j=0}^{\infty} (-1)^m\, m \exp(-xm(2j+1)) \left(2j+1\right)^2.$$

Combining I_1 and I_2 we obtain after some algebra,

$$M_{11} \sim \frac{2\pi^3}{L^2 n^2} \left\{ \sum_{m=1}^{\infty} \sum_{j=1}^{\infty} m\,(-1)^{mj} \exp(-xmj) j^2 \right\} \sim \frac{2\pi^3}{L^2 n^2} \left\{ \sum_{1}^{\infty} j^2 \frac{(-1)^j e^{-xj}}{\left(1 - (-1)^j e^{-xj}\right)^2} \right\} \tag{3.18}$$

From (2.16) we have $M_{22} \sim -\frac{N}{LH}$, and furthermore a similar computation yields $M_{12} = M_{21} = 0$.It follows that the eigenvalues are given by M_{11} and M_{22}. Moreover M_{22} is negative, so the threshold for instability corresponds to the sign change in M_{11}. The equation

$$\sum j^2 \frac{(-1)^j e^{-xj}}{\left(1 - (-1)^j e^{-xj}\right)^2} = 0 \tag{3.19}$$

has a unique root $x = 1.51452 = \frac{H\pi}{LN}$. It follows that the stripe is *stable* if $\frac{H}{LN} \geq a_0$, where $a_0 = x/\pi = 0.482\,09$. This completes the derivation of Proposition 1.2.

4. THRESHOLDS FOR HEXAGONAL LATTICE AND ITS DILATIONS

In this section we consider the stability of the lattice spanned by vectors (1.11) in the limit $N = 2n^2 \to \infty$.. Explicitly, the lattice points are

$$x_j = \frac{L}{n}\left(j_1 + \frac{j_2}{2}\right) \pmod{L}, \quad y_j = \frac{H}{n}\frac{j_2}{2}; \quad j_1 = 0 \dots n-1, \quad j_2 = 0 \dots 2n-1.$$

They forms a perfect hexagonal lattice when $L/H = \sqrt{3}$ or $1/\sqrt{3}$. Let $\rho = L/H$. Numerical experiments (see Figure 4) show that this lattice is stable for a range of aspect ratios as given in Proposition 1.3. Moreover the dominant instability at lower boundary (resp. upper) is due to the mode $(m_1, m_2) = (0, 1)$, (resp. $(n/2, 0)$). The goal here is to compute these thresholds.

Mode $m_1 = 0, m_2 = 1$. We start by computing M_{11} entry in (2.14). Using G_{xx} as given in (A.4) we have

$$M_{11} = -\frac{2\pi}{L^2}\sum_{j_1=0}^{n-1}\sum_{j_2=1}^{2n-1}\sum_{q=1}^{\infty} q\cos\left(\frac{2\pi q}{n}\left(j_1 + \frac{j_2}{2}\right)\right)\frac{\cosh\left(\left(\frac{j_2}{n}-1\right)\frac{\pi}{L}qH\right)}{\sinh\left(\frac{\pi}{L}qH\right)}\left(\exp\left(\pi i j_2/n\right) - 1\right).$$

Note that

$$\sum_{j_1=0}^{n-1}\cos\left(\frac{2\pi q}{n}\left(j_1 + \frac{j_2}{2}\right)\right) = \begin{cases} 0, & n|q \\ n\cos\left(\frac{\pi q}{n}j_2\right), & n \not| q \end{cases}$$

so we let

$$q = Qn, \quad Q = 1, 2, \dots$$

and we obtain

$$M_{11} = -\frac{2\pi}{L^2}n^2\sum_{j_2=1}^{2n-1}\sum_{Q=1}^{\infty} Q\cos\left(\pi Q j_2\right)\frac{\cosh\left(\left(\frac{j_2}{n}-1\right)\frac{\pi}{L}QnH\right)}{\sinh\left(\frac{\pi}{L}QnH\right)}\left(\cos\left(\frac{\pi}{n}j_2\right) - 1\right). \tag{4.20}$$

We further estimate

$$\frac{\cosh\left(\left(\frac{j_2}{n}-1\right)\frac{\pi}{L}QnH\right)}{\sinh\left(\frac{\pi}{L}QnH\right)} \sim \exp\left(-j_2\pi Q\frac{H}{L}\right), \quad j_2 < n$$

In addition the sum over j_2 is symmetric (the contribution from j_2 is the same as contribution from $2n - j_2$). It follows that (4.20) is approximated by

$$M_{11} \sim -\frac{4\pi}{L^2}n^2\sum_{j_2=1}^{\infty}\sum_{Q=1}^{\infty} Q\cos\left(\pi Q j_2\right)\exp\left(-j_2\pi Q\frac{H}{L}\right)\left(\cos\left(\frac{\pi}{n}j_2\right) - 1\right).$$

Finally we expand in Taylor series $\cos\left(\frac{\pi}{n}j_2\right) - 1 \sim -\left(\frac{\pi}{n}j_2\right)^2/2$ to obtain

$$M_{11} \sim \frac{2\pi^2}{L^2}\sum_{j_2=1}^{\infty}\sum_{Q=1}^{\infty} Q\cos\left(\pi Q j_2\right)\exp\left(-j_2\pi\frac{H}{L}Q\right)j_2^2.$$

From (2.16) we have $M_{22} \sim -\frac{N}{LH} + O(1) < 0$. Moreover it is easy to verify that $M_{12} = 0 = M_{12}$. Therefore the threshold is computed by setting $M_{11} = 0$. We remark that this sum is equivalent to the sum appearing in (3.18), and can be rewritten as a single sum using genometric series as done there. Assuming $H/L < 1$, setting $M_{11} = 0$ we obtain $\frac{H}{L} \approx 0.48209$, which is the same constant as derived in Proposition 1.2. This is the lower threshold a_0 of Proposition 1.3.

Mode $m_1 = n/2, \ m_2 = 0$. To simplify the derivaiton, in what follows, we will assume that n is even. However the final formula is also valid for odd n. We start with evaluating M_{11}. We have:

$$M_{11} = \sum_{j_1=1}^{n_1-1}\sum_{j_2=0}^{n_2-1} G_{xx}(x_j, y_j)\left(\exp\left\{\pi i j_1\right\} - 1\right), \quad x_j = \frac{L}{n}\left(j_1 + \frac{j_2}{2}\right) \bmod L, \quad y_j = \frac{H}{n}\frac{j_2}{2}.$$

It turns out that it is necessary to split this sum into $j_2 = 0$ and $j_2 > 1$. For $j_2 = 0$ we will use the expression

$$G_{xx} = \frac{1}{HL} + \frac{2\pi}{H^2}\sum_{q=1}^{\infty} q\cos\left(2\pi q\frac{y}{H}\right)\frac{\cosh\left((x-L/2)\,\frac{2\pi}{H}q\right)}{\sinh\left(\frac{2\pi}{H}qL/2\right)} \tag{4.21}$$

For $j_2 > 0$, we will use instead the expression

$$G_{xx} = -\frac{2\pi}{L^2}\sum_{q=1}^{\infty} q\cos\left(2\pi q\frac{x}{L}\right)\frac{\cosh\left((y-H/2)\,\frac{2\pi}{L}q\right)}{\sinh\left(\frac{2\pi}{L}qH/2\right)}. \tag{4.22}$$

We then write $M_{11} = I_1 + I_2$, where

$$I_1 = -\frac{2\pi}{L^2}\sum_{j_1=1}^{n_1-1}\sum_{j_2=1}^{n_2-1}\sum_{q=1}^{\infty} q\cos\left(2\pi q\frac{\left(j_1+\frac{j_2}{2}\right)}{n}\right)\frac{\cosh\left(\left(\frac{H}{n}\frac{j_2}{2}-H/2\right)\frac{2\pi}{L}q\right)}{\sinh\left(\frac{2\pi}{L}qH/2\right)}\left(\exp\{\pi i j_1\}-1\right)$$

$$I_2 = \sum_{j_1=1}^{n-1}\left\{\frac{1}{HL} + \frac{2\pi}{H^2}\sum_{q=1}^{\infty} q\frac{\cosh\left(\left(\frac{L}{n}j_1 - L/2\right)\frac{2\pi}{H}q\right)}{\sinh\left(\frac{2\pi}{H}qL/2\right)}\right\}\left(\exp\{\pi i j_1\}-1\right).$$

We start with I_1. Let $\hat{n} = n/2$ Summing over j_1 first, we have the following identity:

$$\sum_{j_1=1}^{n-1}\cos\left(2\pi q\frac{\left(j_1+\frac{j_2}{2}\right)}{n}\right)\left(\exp\{\pi i j_1\}-1\right) = -2\sum_{j=0}^{\hat{n}-1}\cos\left(\frac{2\pi q}{\hat{n}}j + \frac{\pi q}{\hat{n}}\left(1+\frac{j_2}{2}\right)\right)$$

$$= \begin{cases} 0, & \hat{n}\not| q \\ -2\hat{n}\cos\left(\frac{\pi q}{\hat{n}}\left(1+\frac{j_2}{2}\right)\right), & \hat{n}|q \end{cases}$$

Let $q = Q\hat{n}$. Then $\cos\left(\frac{2\pi q}{n}\left(1+\frac{j_2}{2}\right)\right) = \cos\left(\pi Q\left(1+\frac{j_2}{2}\right)\right)$ and we obtain the asymptotics

$$I_1 = n\frac{2\pi}{L^2}\sum_{j_2=1}^{n_2-1}\sum_{Q=1}^{\infty}\frac{Q}{2}n\frac{\cosh\left(\left(\frac{H}{n}\frac{j_2}{2}-H/2\right)\frac{\pi}{L}Qn\right)}{\sinh\left(\frac{\pi}{L}QnH/2\right)}\cos\left(\pi Q\left(1+\frac{j_2}{2}\right)\right)$$

$$\sim n^2\frac{2\pi}{L^2}\sum_{j_2=1}^{\infty}\sum_{Q=1}^{\infty} Q\exp\left(-H\frac{\pi}{L}jQ\right)\cos\left(\pi Q\left(1+\frac{j_2}{2}\right)\right).$$

Next we evaluate I_2. Start by rewriting $j_1 = 2k+1, \quad \hat{n} = n/2$, to obtain

$$I_2 = -2\sum_{k=0}^{\hat{n}-1}\left\{\frac{1}{HL} + \frac{2\pi}{H^2}\sum_{q=1}^{\infty} q\frac{\cosh\left(\left(\frac{L}{n}(2k+1) - L/2\right)\frac{2\pi}{H}q\right)}{\sinh\left(\frac{2\pi}{H}qL/2\right)}\right\}$$

$$\sim -\frac{n}{HL} - \frac{4\pi}{H^2}\sum_{k=0}^{\hat{n}-1}\sum_{q=1}^{\infty} q\frac{\cosh\left(aq\left(1-\frac{2k}{\hat{n}}-\frac{1}{\hat{n}}\right)\right)}{\sinh(aq)}$$

where we defined

$$a := \frac{\pi}{H}L.$$

We re-sum the inner sum as follows. Suppose $|b| < a$. Then we have

$$\sum_{q=1}^{\infty} q\frac{\cosh(bq)}{\sinh(aq)} = \sum_{q=1}^{\infty} q\left(e^{bq}+e^{-bq}\right)\left(1-e^{-2aq}\right)^{-1}e^{-aq}$$

$$= \sum_{p=0}^{\infty}\sum_{q=1}^{\infty} q\left(e^{-(2ap+a-b)q} + e^{-(2ap+a+b)q}\right)$$

$$= \sum_{p=0}^{\infty}\frac{e^{-(2ap+a-b)}}{\left(1-e^{-(2ap+a-b)}\right)^2} + \frac{e^{-(2ap+a+b)}}{\left(1-e^{-(2ap+a+b)}\right)^2}$$

$$= \sum_{p=0}^{\infty}\frac{1}{4\sinh^2\left(ap+\frac{a-b}{2}\right)} + \frac{1}{4\sinh^2\left(ap+\frac{a+b}{2}\right)}$$

We then obtain:

$$\sum_{k=0}^{\hat{n}}\sum_{q=1}^{\infty} q\frac{\cosh\left(aq\left(1-\frac{2k}{\hat{n}}-\frac{1}{\hat{n}}\right)\right)}{\sinh\left(aq\right)} = \sum_{p=0}^{\infty}\sum_{k=0}^{\hat{n}-1}\frac{1}{4\sinh^2\left(ap+a\left(\frac{k}{\hat{n}}+\frac{1}{2\hat{n}}\right)\right)}+\frac{1}{4\sinh^2\left(ap+a\left(1-\frac{k}{\hat{n}}-\frac{1}{2\hat{n}}\right)\right)}$$
$$= \sum_{p=0}^{\infty}\sum_{k=0}^{\hat{n}-1}\frac{1}{2\sinh^2\left(ap+a\left(\frac{k}{\hat{n}}+\frac{1}{2\hat{n}}\right)\right)}$$

We split the last sum into two:

$$= \sum_{k=0}^{\hat{n}-1}\frac{1}{2\sinh^2\left(a\left(\frac{k}{\hat{n}}+\frac{1}{2\hat{n}}\right)\right)}+\sum_{p=1}^{\infty}\sum_{k=0}^{\hat{n}-1}\frac{1}{2\sinh^2\left(ap+a\left(\frac{k}{\hat{n}}+\frac{1}{2\hat{n}}\right)\right)}.$$

For $p>0$ we can estimate the inner sum by an integral as follows:

$$\sum_{k=0}^{\hat{n}-1}\frac{1}{2\sinh^2\left(ap+a\left(\frac{k}{\hat{n}}+\frac{1}{2\hat{n}}\right)\right)} \sim \frac{\hat{n}}{2a}\int_0^a \frac{dy}{\sinh^2\left(ap+y\right)}$$
$$\sim \frac{\hat{n}}{2a}\left[\coth(ap)-\coth(ap+a)\right].$$

It follows that

$$\sum_{p=1}^{\infty}\sum_{k=0}^{\hat{n}-1}\frac{1}{2\sinh^2\left(ap+a\left(\frac{k}{\hat{n}}+\frac{1}{2\hat{n}}\right)\right)} \sim \frac{\hat{n}}{2a}\left[\coth(a)-1\right].$$

For $p=0$, at leading order we use series expansion $\sinh(z)\sim z$ to we estimate, to leading order,

$$\sum_{k=0}^{\hat{n}-1}\frac{1}{2\sinh^2\left(a\left(\frac{k}{\hat{n}}+\frac{1}{2\hat{n}}\right)\right)} \sim \frac{n^2}{2a^2}\sum_0^{n-1}\frac{1}{(k+1/2)^2} \sim \frac{n^2}{2a^2}\sum_0^{\infty}\frac{1}{(k+1/2)^2} \sim \frac{n^2}{2a^2}\frac{\pi}{2}.$$

However we will need a two-order expansion to accurately compute the eigenvalue threshold. So we extract the singularity to compute as follows:

$$\sum_{k=0}^{\hat{n}-1}\frac{1}{2\sinh^2\left(a\left(\frac{k}{\hat{n}}+\frac{1}{2\hat{n}}\right)\right)} \sim \sum_{k=0}^{\hat{n}-1}\frac{1}{2\sinh^2\left(a\left(\frac{k}{\hat{n}}+\frac{1}{2\hat{n}}\right)\right)}-\frac{1}{2\left(a\left(\frac{k+1/2}{\hat{n}}\right)\right)^2}+\frac{1}{2\left(a\left(\frac{k+1/2}{\hat{n}}\right)\right)^2}$$
$$\sim \frac{\hat{n}^2}{2a^2}\sum_0^{\hat{n}-1}\frac{1}{(k+1/2)^2}+\int_0^{\hat{n}-1}\frac{1}{2\sinh^2\left(a\left(\frac{k}{\hat{n}}+\frac{1}{2\hat{n}}\right)\right)}-\frac{1}{2\left(a\left(\frac{k+1/2}{\hat{n}}\right)\right)^2}$$
$$\sim \frac{\hat{n}^2}{2a^2}\left[\frac{\pi}{2}-\int_{\hat{n}}^{\infty}\frac{dk}{(k+1/2)^2}\right]+\int_0^{\hat{n}-1}\frac{1}{2\sinh^2\left(a\left(\frac{k}{\hat{n}}+\frac{1}{2\hat{n}}\right)\right)}-\frac{1}{2\left(a\left(\frac{k+1/2}{\hat{n}}\right)\right)^2}$$
$$\sim \frac{\hat{n}^2}{2a^2}\left[\frac{\pi}{2}-\frac{1}{(\hat{n}+1/2)}\right]+\frac{1}{2}\frac{\hat{n}}{a}\int_0^a\left(\frac{1}{\sin^2 y}-\frac{1}{y^2}\right)dy$$
$$\sim \frac{\hat{n}^2\pi}{4a^2}-\frac{1}{2}\frac{\hat{n}}{a}\coth a$$

In summary, we obtain a two-order expansion

$$\sum_{k=0}^{n/2-1}\sum_{q=1}^{\infty} q\frac{\cosh\left(aq\left(1-\frac{2k}{\hat{n}}-\frac{1}{\hat{n}}\right)\right)}{\sinh\left(aq\right)} \sim \frac{\hat{n}^2\pi^2}{4a^2}-\frac{\hat{n}}{2a}.$$

Putting all the parts for I_2 we finally obtain $I_2 \sim -\frac{\pi n^2}{4L^2}$.

$$M_{11} = -\frac{\pi n^2}{4L^2} + n^2 \frac{2\pi}{L^2} \sum_{j_2=1}^{\infty} \sum_{Q=1}^{\infty} Q \exp\left(-H j_2 \frac{\pi}{2L} Q\right) \cos\left(\pi Q \left(1 + \frac{j_2}{2}\right)\right)$$

From (2.16) we have $M_{22} = -\frac{2n^2}{LH} - M_{11}$.The term M_{12} is evaluated similarly. We summize the computations as follows. Let $\rho = H/L$ and let

$$f_1(\rho) = \sum_{j=1}^{\infty} \sum_{Q=1}^{\infty} Q \exp\left(-j \frac{\pi}{2} \rho Q\right) \cos\left(\pi Q \left(1 + \frac{j}{2}\right)\right) \tag{4.23}$$

$$f_2(\rho) = \sum_{j=1}^{\infty} \sum_{Q=1}^{\infty} Q \exp\left(-j \frac{\pi}{2} \rho Q\right) \sin\left(\pi Q \left(1 + \frac{j}{2}\right)\right) \tag{4.24}$$

Then

$$\begin{aligned} M_{11} &= n^2 \frac{2\pi}{L^2} \left(f_1(\rho) - \frac{1}{8}\right) \\ M_{22} &= n^2 \frac{2\pi}{L^2} \left(-f_1(\rho) + \frac{1}{8} - \frac{1}{\pi\rho}\right) \qquad (4.25) \\ M_{12} &= -n^2 \frac{2\pi}{L^2} f_2(\rho). \qquad (4.26) \end{aligned}$$

In particular the threshold is obtained by setting $\det(M) = 0$. This yields the following formula for ρ,

$$\left(f_1(\rho) - \frac{1}{8}\right)\left(-f_1(\rho) + \frac{1}{8} - \frac{1}{\pi\rho}\right) - f_2^2(\rho) = 0 \tag{4.27}$$

Solving for ρ with $0 < \rho < 1$, we get $\rho = H/L = 0.767837$, corresponding to the angle of 37.52 degrees.

5. REACTION-DIFFUSION SYSTEMS, LARGE EIGENVALUES

Many RD systems generate spot patterns. One of the simplest is the Schnakenberg model (1.3). The analysis for a general bounded two-dimensional domain for this and other models is well established; see for example [11, 12, 17]. Here, we will adapt the results from [1] which deals with ring-type spot patterns for the Schnakenberg model (1.3). Most of the analysis is the same for lattice patterns, so we will not re-derive all the results, but only present the formulas modified for the case of lattice patterns.

As is well known, there are two types of instabilities that are possible: due to large ($O(1)$) or small ($O(\varepsilon^2)$) eigenvalues. Instability triggered by large eigenvalues induces a "structural" or spike profile instability on an O(1) time scale. Small eigenvalues arise from near translation-invariance of spikes. To leading order, spot dynamics is governed (up to time-scaling) by the gradient flow (1.6). Stable equilibria of this ODE system correspond to equilibrium spot locations of the original model. As such, the domain shape (e.g. aspect ratio) is responsible for destabilization of the small eigenvalues. A small-eigenvalue instability can lead to re-arrangement of the spots while preserving the overall number of spots. This is illustrated in Figure 4(e,f); detailed analysis of this situation is given in §4.

On the other hand, a large-eigenvalue instability, also called a competition instability, leads to a reduction in the number of spikes. It is triggered when the feed-rate A is decreased past a certain threshold. Figure 5 illustrates this phenomenon. We start with random initial conditions, using parameters as given in the figure. Very quickly, a spot pattern emerges. After further self-replication, the system settles to a stable equilibrium consisting of 24 spots. This corresponds to the stable lattice with $N = 24 = 24 \times 1$ generated by a single generator $(1, 5)$ (see Figure 5(c)). Next, we start to decrease A. The pattern was found to be stable when $A = 40$, but instability occurs when $A = 39$. As a result of the instability, 8 spots are destroyed resulting in a honeycomb-type lattice. This state appears to be transient although it persists for a rather long time: presumably the honeycomb state is a saddle critical point of the energy E. After some time the system settles into an $N = 16$ stable lattice.

These competition thresholds, as well as the shape of the resulting instability, can be computed analytically in the case of a lattice, as we now show. Equation (28) from [1] gives the formula for the competition instability thresholds

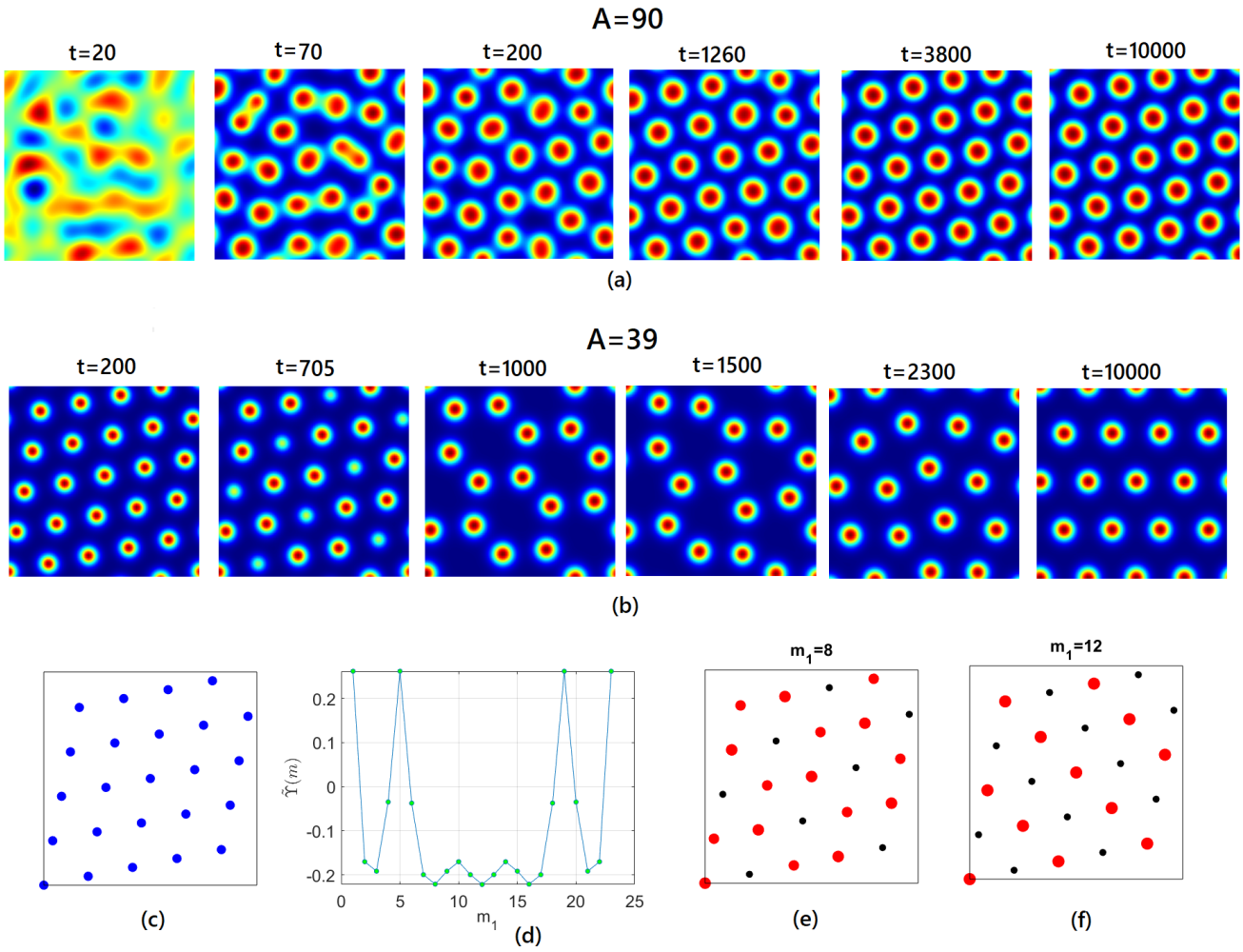

FIG. 5. (a) Simulation of (1.3) starting with random initial conditions. The parameter values are $\Omega = (0,2) \times (0,2)$; $A = 90$, $\varepsilon = 0.04$. After some complicated transient dynamics the system settles to the unique stable regular lattice pattern with 24 spots. (b) Simulation with $A = 39$, using final output of (a) as the initial condition. A competition instability eventually results in a death of 8 spots and the system transitions to a honeycomp-like equilibrium of 16 spots. This equilibrium is eventually destabilized and the final steady state is a unique stable regular lattice of 16 spots. (c) Stable 24-point regular lattice generated by the vector $(1,5)$. (d) Plot of $\tilde{\Upsilon}(m)$ as a function of $m = (m_1, 0)$. (e) Instability due to mode $m_1 = 8$. Here, $\phi_k = \cos(2\pi m/N) + \sin(2\pi m/N)$; black dots correspond to $\phi_k < 0$ and red dots correspond to $\phi_k > 0$. (f) Instability due to mode $m_2 = 12$.

of a ring of spots inside a disk. The derivation is identical for a lattice with small modifications. We skip the details and just state final result here. There are a total of $N-1$ instabilitity thresholds, characterized by $N-1$ modes $m = (m_1, m_2)$ with $m \neq (0,0)$. These thresholds can are given, asymptoitcally, as follows.

Define

$$A_0 = \frac{1}{\log \varepsilon^{-1}} \frac{N}{|\Omega|} \left(2\pi \int w^2 \right)^{1/2}. \tag{5.28}$$

Given $m = (m_1, m_2) \neq (0,0)$, define

$$A_m := A_0 \left(1 + \frac{2\pi}{\log \varepsilon^{-1}} \tilde{\Upsilon}(m) \right)^{-1/2} \tag{5.29}$$

where

$$\tilde{\Upsilon}(m) = \sum_{l \neq 0} \exp\left\{ 2\pi i \left(\frac{m_1}{n_1} l_1 + \frac{m_2}{n_2} l_2 \right) \right\} G(vl) + R_0. \tag{5.30}$$

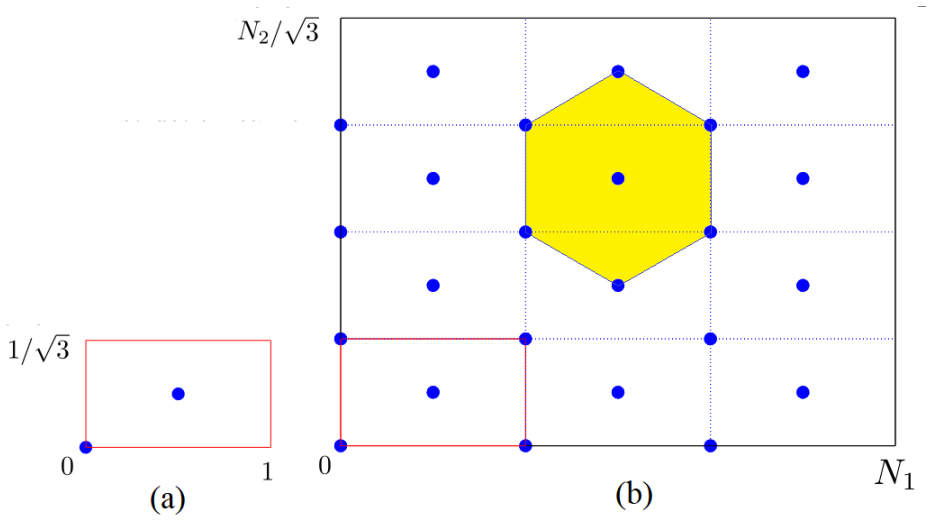

FIG. 6. General construction of a perfect hexagonal lattice without defects. (a) Start with a rectangle whose aspect ratio is $\sqrt{3}$, and with two particles, one at the center another at the corner. (b) Copy the rectangle N_1 times horizontally and then N_2 times vertically. The result is a perfect hexagonal lattice with $N = 2N_1N_2$ particles (here, the case of $N_1 = 3,\ N_2 = 4$ is shown).

Here, R_0 is the regular part of G, given by $R_0 = \lim_{x\to 0}\left(G(x) + \frac{1}{2\pi}\log|x|\right)$ .The formula for R_0 is given in Appendix A, see (A.5). The threshold A_m is the instability threshold corresponding to the mode m; it is stable if $A > A_m$ and becomes unstable as A is decreased below A_m. The overall threshold is then given by

$$A_{\max} = \max_m (A_m)\,; \tag{5.31}$$

it occurs at the minimum of $\tilde{\Upsilon}(m)$. The corresponding destabilizing eigenvector has the form $\phi_k = A\cos\left(\frac{2\pi}{N}m\cdot k\right) + B\cos\left(\frac{2\pi}{N}m\cdot k\right)$. The height of k-th spot is perturbed by ϕ_k, thus initiating the instability. The spots where $\phi_k < 0$ decrease in height and those where $\phi_k > 0$ increase in height. Because competition instability is typically subcritical (see [18] for related analysis), it eventually this leads to death of those spots for which $\phi_k < 0$. Moreover, the instability-inducing eigenfunction (responsible for competition instability) corresponds to the the mode $m = (m_1, m_2)$ which minimizes $\tilde{\Upsilon}(m)$. In other words, spot heights $u_k = u(x_k)$ at the lattice locations $x_k = vk$ are perturbed by an amount proportional to ϕ_k.

Figure 5 provides a test case of the theory. The steady state here consists of 24 spots arranged on a regular lattice of the form (1.7) with $v_1 = (1, 5),\ v_2 = 0$. The function $\tilde{\Upsilon}(m)$ is shown in Figure 5(d) and we find that $\min_m \tilde{\Upsilon}(m) = -0.2218$; the minimizing mode is $m = (12, 0)$. To leading order, the instability threshold (5.28) does not depend on this perturbation; we find its numerical value to be $A_0 \approx 26.0$. More precise value of $A_{\max} \approx 34.6$ incorporates the modes m. Full simulations of the PDE (1.3) show that the *actual* onset of the instability happens at around $A \approx 39$; this is reasonably close to the predicted value of $A_{\max}$. However the instability that is triggered appears to to correspond to the mode $m = (8, 0)$, not $(12, 0)$. In fact, $\tilde{\Upsilon}(8, 0) = -0.2211$, only 0.3% above the minimum of -0.2218.

6. DISCUSSION

Regular lattice patterns are prevalent in many pattern-forming systems. We have presented detailed analysis of classification and stability of such patterns on periodic rectangular domains. We used explicit computations of the aassociated Green's function as well as numerical experiments to explcitly characterize stability boundaries of hexagonal-type patterns, as the domain is stretched or compressed. There are many open questions that remain.

When the rectangle is a square, explicit classification showed that there is no stable lattice when $N = 6, 7, 13, 21...$ It would be interesting to study the shape of the minimizer of (1.5) in these cases, even with $N = 6$. It is also an open question whether these gaps persist even for larger N.

We showed that a specific hexagonal lattice in Proposition 1.3 is stable. This construction can be generalized as follows. Start with a rectangle with aspect ratio of l, h containing exactly 2 particles: one at the center and one at the

corner. Make N_1 copies horizontally. Then make N_2 copies vertically, as illustrated in Figure 6 with $N_1 = 3,\ N_2 = 4$. The resulting rectangle has $N = 2N_1N_2$ particles and the aspect ratio of $\frac{lN_1}{hN_2}$. The resulting lattice is a perfect hexagonal lattice when $l/h = \sqrt{3}$. We verified numerically that this lattice is stable for all N_1, N_2 up to 10. In fact we conjecture that it is stable in the limit $N_1, N_2 \to \infty$ as long as $h/l \in (a_0, a_1)$ as in Proposition 1.3.

Numerical optimization and gradient flow experiments shows that stable regular lattices are often global minimizers. Further experimentation suggests that whenever there is an admissable hexagonal lattice without any defects (such as constructed above), it will be a global minimum. We propose this as a conjecture.

Conjecture. Given two integers N_1, N_2, suppose that $N = 2N_1N_2$, and $L/H = \sqrt{3}N_1/N_2$. Then the global minimizer of (1.5) is a perfect hexagonal lattice such as shown in Figure 6.

It would be interesting to see how changing the pairwise function G changes the results. For example, many reaction-diffusion systems require the Green's function with decay, $\Delta G - G + \delta(x) = 0$. Another generalization is to use a fractional Laplacian. While the spectral decomposition in §2 is generic (independent on the specific form of G), the stability of lattices for different aspect ratios will change. It would be interesting to use the framework in this paper to generalize our results to these cases.

Appendix A: Periodic Green's function

The periodic Green's function G on the rectangle $\Omega = (0, L) \times (0, H)$ satisfies

$$G_{xx} + G_{yy} - \frac{1}{LH} + \delta(x)\delta(y) = 0, \quad G \text{ periodic on } \Omega, \quad \iint_\Omega G = 0.$$

Expand:

$$G = \frac{u_0(x)}{2} + \sum_{m=1}^{\infty} \cos\left(y\frac{2\pi}{H}m\right) u_m(x); \tag{A.1}$$

$$\delta(x)\delta(y) = \delta(x)\left(\frac{1}{H} + \sum_{m=1}^{\infty} \cos\left(y\frac{2\pi}{H}m\right)\frac{2}{H}\right); \tag{A.2}$$

Then $u_m,\ m > 0$ satisfies:

$$(u_m)_{xx} - \alpha_m^2 u_m + \frac{2}{H}\delta(x) = 0; \quad \alpha_m = \frac{2\pi}{H}m;$$

whose solution is given by

$$u_m(x) = \frac{\cosh\left((x - L/2)\,\alpha_m\right)}{H\alpha\sinh\left(\alpha L/2\right)},$$

whereas u_0 satisfies

$$u_{0xx} - \frac{2}{LH} + \frac{2}{H}\delta(x) = 0$$

so that $u_0 = \frac{1}{HL}(x - L/2)^2 + C$; C is an integration constant, chosen to make $\iint_\Omega G = 0$, that is, $LC = -\frac{1}{HL}\int_0^L (x - L/2)^2\,dx$. In summary, we obtain

$$G = -\frac{L}{24H} + \frac{1}{2HL}(x - L/2)^2 + \sum_{m=1}^{\infty} \cos\left(2\pi m\frac{y}{H}\right)\frac{\cosh\left((x - L/2)\,\frac{2\pi}{H}m\right)}{2\pi m\sinh\left(\frac{\pi}{H}mL\right)} \tag{A.3}$$

$$= -\frac{H}{24L} + \frac{1}{2HL}(y - H/2)^2 + \sum_{m=1}^{\infty} \cos\left(2\pi m\frac{x}{L}\right)\frac{\cosh\left((y - H/2)\,\frac{2\pi}{L}m\right)}{2\pi m\sinh\left(\frac{\pi}{L}mH\right)}. \tag{A.4}$$

Formula (A.4) is obtained due to symmetry in exchaning $x \leftrightarrow y,\ L \leftrightarrow H$. Formula (A.3) is convergent for $x \neq 0$ whereas (A.4) is convergent for $y \neq 0$, and both are used in our analysis.

Finally, section 5 requires the regular part of the Green's function. This is defined as

$$R(x, y) = G(x, y) + \frac{1}{2\pi}\log\sqrt{x^2 + y^2}$$

and in particular we need $R_0 = \lim_{(x,y)\to(0,0)} R(x,y)$. This computation involves a resummation trick. We refer the reader to formulas (4.14) from [17], where this expression is derived for a rectangle with Neumann boundary coditions. The periodic case is a special case of (4.14) where the source is taken to be the center of the rectangle. After some algebra, formula (4.14) from [17] then simplifies to

$$R_0 = \frac{H}{12L} - \frac{1}{2\pi}\log\left(\frac{2\pi}{L}\right) - \frac{1}{\pi}\sum_{n=1}^{\infty}\log\left(1-\exp\left(-\frac{2\pi H}{L}n\right)\right). \tag{A.5}$$

Appendix B: Catalogue of integer lattices and their stability

The number of distinct integer lattices on a square has a generating function (1.9) which was derived in [15]. To study lattice stability we actually need to construct them first. Here, we describe an algorithm to do this. It is implemented in Matlab program which is available from the authors [16]. Before describing an algorithm, we give some definitions and theory.

Define a *lattice generated by a single generator* (a,b) to be the lattice $\{(a,b)j \pmod N, \quad j \in \mathbb{Z}_N\}$. We call such a generator (or lattice) $N-$*admissable* if there are exactly N distinct values in this set. For example, the generator (4,6) is 9-admissable but is not 10-admissable (since $4\times 5, 6\times 5 \equiv 0 (\mathrm{mod}\, 10)$).

Similary a *lattice generated by a double generator* $(a,b),(c,d)$ is given by (1.7); it is $N-$*admissable* if it has size N. The key observation is that for a double-generator lattice to be admissable, (a,b) must be a single-generator n_1-admissable and (c,d) must be a single-generator n_2-admissable. This reduces the complexity of generating all possible lattices significantly.

We call two sets of generators isomorphic if they generate identical lattices. Besides the algebraic isomorphism, there is also a geometric equivalence. For a square, we define two lattices to be *equivalent* if one can be obtained from the other by either rotation by 90 degrees or a flip; otherwise call them non-equivalent (for a non-square rectangle, only rotation by 180 degrees and flips are allowed). Each single generator can generate up to four different but equivalent square lattices: (a,b), (b,a), $(a,-b)$ and $(-a,b)$.

The algorithm to generate all non-equivalent lattices is as follows.

- For each distinct factorization $N = n_1 n_2$:
  - Generate all non-isomorphic single-generator lattices of sizes n_1 and n_2.
  - Generate all double-generator lattices of the form $(a,b),(c,d)$ where (a,b) is n_1-admissable and (c,d) is n_2-admissable single-generator lattice.
- Select non-equivalent lattices from the resulting list.

To generate all single-generator lattices, we use the following facts. Signle-generators $v=(a,b)$ and $w=(c,d)$ are isomorphic if and only if $(a,b) = x(c,d)$ for some invertible element $x \in \mathbb{Z}_N$. In particular, if c is invertible, then (a,b) is isomorphic to $\left(1, a^{-1}b\right)$. When N is a prime, any signle-generator is isomorphic to either $(1,x)$ for some x, or to $(0,1)$. The following fact further reduces the search space: a single generator (a,b) is $N-$admissable if and only if $\gcd(a,b,N)=1$.

The last step requires an equivalence/isomorphism checking for a list of lattices. To do so, for each lattice in the list, we create a unique signture as follows. First, generate a list all point for each lattice as well as admissable geometric reflections/flips (four lists in total for each lattice in case of a square, two lists for a rectangle). Convert each list to a string that consists of points sorted by by their x-coordinates followed by their y-coordinates. Sort the resulting strings and pick the first one. This will correspond to the lattice signature. Finally, uniquefy the list according to lattice signatures.

Table of all lattices up to $N = 200$

The following table summarizes the overall number of non-equivalent lattices on a square, as well as the number of stable lattices up to $N = 200$.

N	#all	#stable	N	#all	#stable	N	#all	#stable	N	#all	#stable	N	#all	#stable
1	1	1	41	12	0	81	33	3	121	35	2	161	50	3
2	2	1	42	28	2	82	34	2	122	49	2	162	96	6
3	2	1	43	12	1	83	22	1	123	44	2	163	42	3
4	4	1	44	25	0	84	64	3	124	60	3	164	78	4
5	3	1	45	23	3	85	30	1	125	42	2	165	76	5
6	5	0	46	20	1	86	35	3	126	84	4	166	65	2
7	3	0	47	13	1	87	32	1	127	33	3	167	43	2
8	7	1	48	39	2	88	51	2	128	71	3	168	132	6
9	5	1	49	16	1	89	24	0	129	46	2	169	48	2
10	7	1	50	27	2	90	65	5	130	68	2	170	86	5
11	4	1	51	20	0	91	30	2	131	34	3	171	68	0
12	11	1	52	29	2	92	46	1	132	92	5	172	81	4
13	5	0	53	15	2	93	34	2	133	42	1	173	45	3
14	8	1	54	34	1	94	38	3	134	53	3	174	94	4
15	8	1	55	20	0	95	32	2	135	64	3	175	65	5
16	12	1	56	36	2	96	73	3	136	74	3	176	101	6
17	6	1	57	22	1	97	26	1	137	36	3	177	62	4
18	13	1	58	25	1	98	46	2	138	76	4	178	70	3
19	6	1	59	16	2	99	42	2	139	36	3	179	46	2
20	15	1	60	50	3	100	61	4	140	92	6	180	149	7
21	10	0	61	17	1	101	27	1	141	50	3	181	47	2
22	11	1	62	26	1	102	58	2	142	56	2	182	88	5
23	7	1	63	29	3	103	27	1	143	44	3	183	64	3
24	21	2	64	38	4	104	59	3	144	113	8	184	96	3
25	10	1	65	24	0	105	52	2	145	48	0	185	60	4
26	13	0	66	40	2	106	43	4	146	58	2	186	100	6
27	12	1	67	18	1	107	28	1	147	60	2	187	56	4
28	18	2	68	36	3	108	78	3	148	71	5	188	88	4
29	9	0	69	26	2	109	29	1	149	39	4	189	84	5
30	22	2	70	40	3	110	58	4	150	99	4	190	94	6
31	9	0	71	19	0	111	40	2	151	39	3	191	49	2
32	21	1	72	58	4	112	70	2	152	81	2	192	139	6
33	14	1	73	20	1	113	30	2	153	62	5	193	50	1
34	16	1	74	31	1	114	64	4	154	76	5	194	76	4
35	14	2	75	34	2	115	38	3	155	50	1	195	88	5
36	29	2	76	39	3	116	57	3	156	106	6	196	106	7
37	11	0	77	26	3	117	49	6	157	41	2	197	51	0
38	17	2	78	46	1	118	47	1	158	62	2	198	123	5
39	16	2	79	21	1	119	38	0	159	56	3	199	51	2
40	29	2	80	55	3	120	102	8	160	105	4	200	126	6

Lattice gallery.

Here we show all non-equivalent lattices for a unit square, for small values of N up to 30. The title shows the basis of each lattice. A single-basis lattice is shown as $N : (ab)$, meaning all points of the form $(a, b)\frac{j}{N} (\mathrm{mod}\, 1), j = 0 \ldots N-1$. A double-basis lattice is shown as $n_1 \times n_2 : (ab), (c, d)$ meaning all points of the form $(a, b)\frac{j_1}{n_1} + (c, d)\frac{j_2}{n_2} (\mathrm{mod}\, 1), j_1 = 0 \ldots n_1 - 1, j_2 = 0 \ldots n_2 - 1$.

The subtitle $E, \lambda_{\max}$ shows the energy $E = \sum \sum_{k \neq j} G(x_k, x_j)$, as well $\lambda_{\max}$, the maximum nonzero eigenvalue of the negative of the hessian of E. A lattice is stable if $\lambda_{\max}$ is negative. For each N, the lattices are sorted by their energy, from minimum to maximum. Stable lattices are shown in blue; unstable in orange.

N=2

2: (1 1)
-0.055159; -0.9994

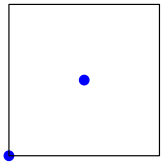

2: (1 0)
-0.027579; 1.189

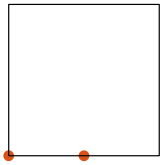

N=3

3: (1 1)
-0.11797; -0.2085

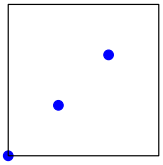

3: (1 0)
-0.013169; 3.32

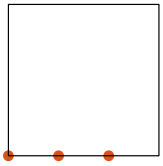

N=4

4: (1 2)
-0.22301; -0.1863

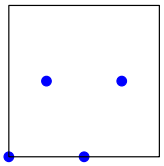

2x2: (1 0), (0 1)
-0.22064; 0.1892

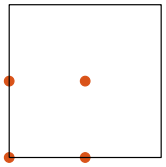

4: (1 1)
-0.16548; 2.371

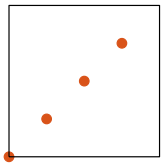

4: (1 0)
0.057537; 8.565

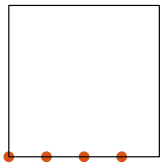

N=5

5: (1 2)
-0.32019; -0.8626

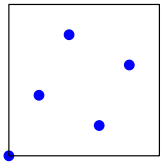

5: (1 1)
-0.19147; 4.481

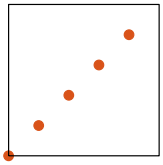

5: (1 0)
0.19147; 13.85

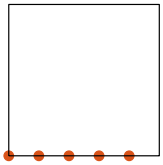

N=6

6: (1 2)
-0.42348; 0.1533

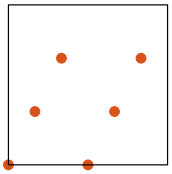

6: (1 3)
-0.40141; 1.075

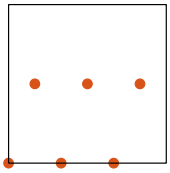

6: (2 3)
-0.40126; 1.198

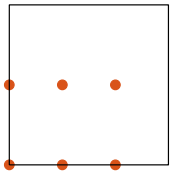

6: (1 1)
-0.19181; 8.125

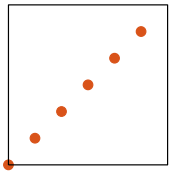

6: (1 0)
0.39271; 22.27

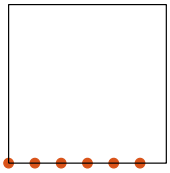

N=7

7: (1 2)
-0.52106; 0.5503

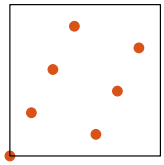

7: (1 1)
-0.16382; 11.84

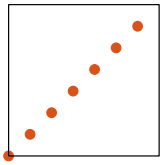

7: (1 0)
0.66396; 30.7

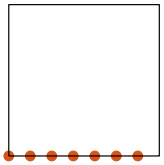

N=8

8: (1 3)
-0.66666; -0.3769

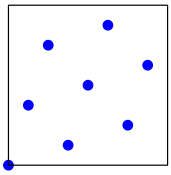

4x2: (1 1), (0 1)
-0.66191; 0.3747

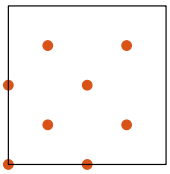

8: (1 2)
-0.61388; 1.758

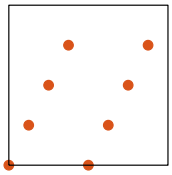

8: (1 4)
-0.5516; 4.565

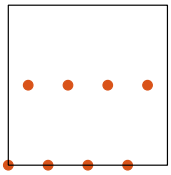

4x2: (1 0), (0 1)
-0.55159; 4.753

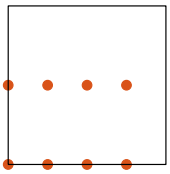

8: (1 1)
-0.10556; 17.15

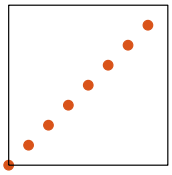

8: (1 0)
1.0071; 42.27

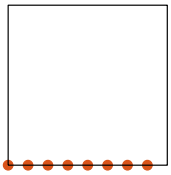

N=9

9: (1 3)
-0.79085; -0.1575

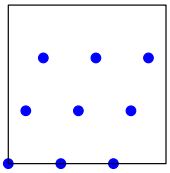

3x3: (1 0), (0 1)
-0.78682; 0.3209

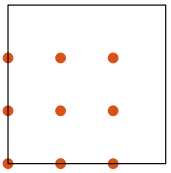

9: (1 2)
-0.70001; 3.433

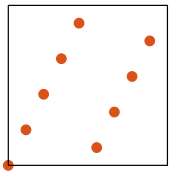

9: (1 1)
-0.015614; 22.42

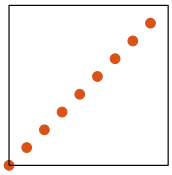

9: (1 0)
1.4237; 53.83

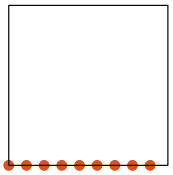

N=10

10: (1 3)
-0.91617; -0.3706

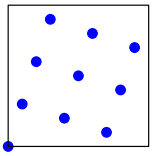

10: (1 4)
-0.90377; 0.8511

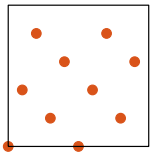

10: (1 2)
-0.77827; 5.948

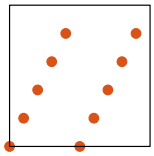

10: (1 5)
-0.65873; 8.962

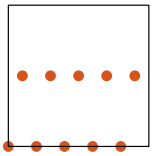

10: (2 5)
-0.65873; 8.974

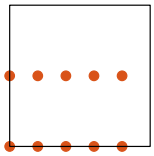

10: (1 1)
0.10714; 29.27

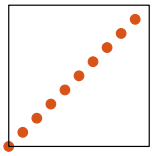

10: (1 0)
1.9147; 68.54

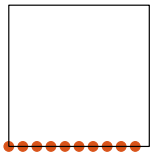

N=11

11: (1 3)
-1.0492; -0.4834

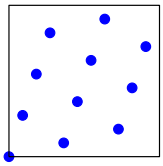

11: (1 2)
-0.84787; 7.948

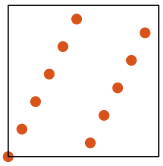

11: (1 1)
0.26359; 36.12

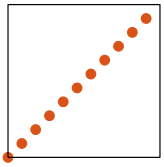

11: (1 0)
2.4811; 83.25

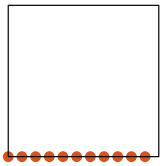

N=12

12: (2 3)
-1.1946; -0.7655

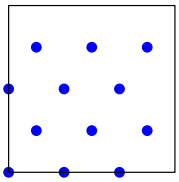

12: (1 3)
-1.1779; 0.2906

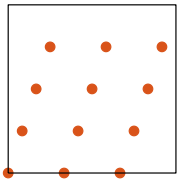

12: (1 4)
-1.1609; 1.001

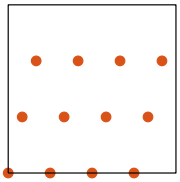

12: (3 4)
-1.1603; 2.066

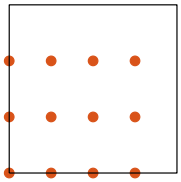

6x2: (1 1), (0 1)
-1.1338; 2.209

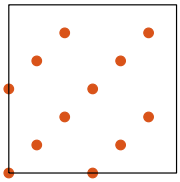

12: (1 5)
-1.1335; 2.392

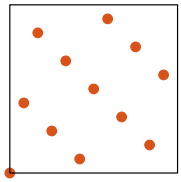

12: (1 2)
-0.90804; 10.54

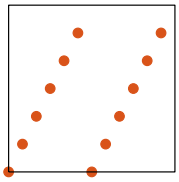

12: (1 6)
-0.71458; 16.27

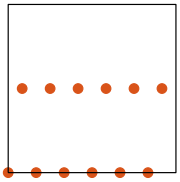

6x2: (1 0), (0 1)
-0.71458; 16.29

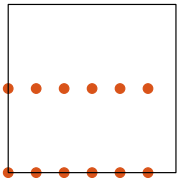

12: (1 1)
0.45447; 44.54

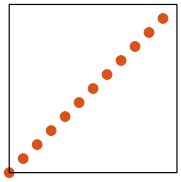

12: (1 0)
3.1235; 101.1

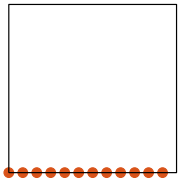

N=13

13: (1 5)
-1.3267; 0.03794

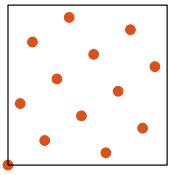

13: (1 3)
-1.3033; 1.067

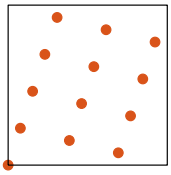

13: (1 2)
-0.95818; 13.35

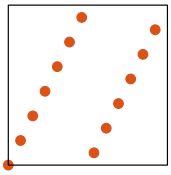

13: (1 1)
0.68037; 52.97

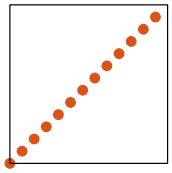

13: (1 0)
3.8427; 118.9

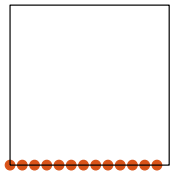

N=14

14: (1 4)
-1.4726; -0.6849

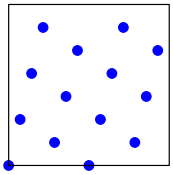

14: (1 3)
-1.4282; 2.652

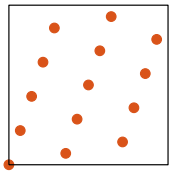

14: (1 6)
-1.3485; 5.022

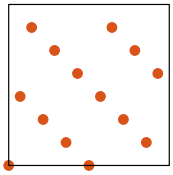

14: (1 2)
-0.99778; 16.8

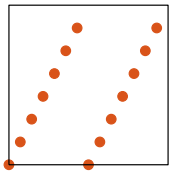

14: (1 7)
-0.71375; 23.71

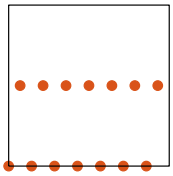

14: (2 7)
-0.71375; 23.71

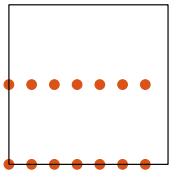

14: (1 1)
0.94181; 62.96

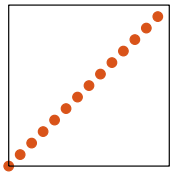

14: (1 0)
4.639; 139.9

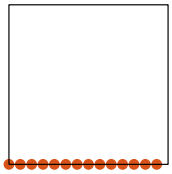

N=15

15: (1 4)
-1.6287; -0.6649

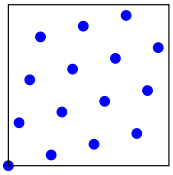

15: (1 6)
-1.6098; 0.6907

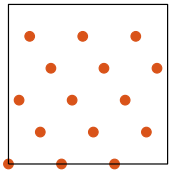

15: (1 3)
-1.5504; 2.908

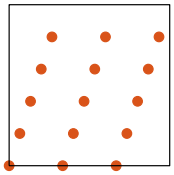

15: (1 5)
-1.509; 4.736

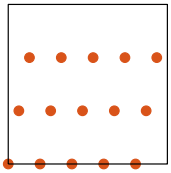

15: (3 5)
-1.5089; 4.987

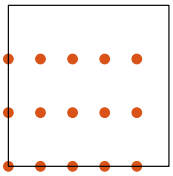

15: (1 2)
-1.0264; 20.19

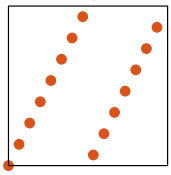

15: (1 1)
1.2392; 72.96

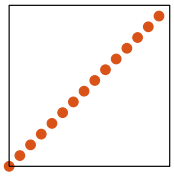

15: (1 0)
5.513; 160.9

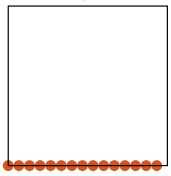

N=16

8x2: (1 2), (0 1)
-1.7746; -0.3244

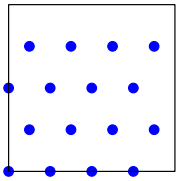

16: (1 4)
-1.7699; 0.03227

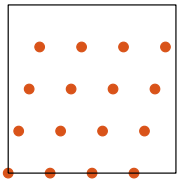

4x4: (1 0), (0 1)
-1.7651; 0.7451

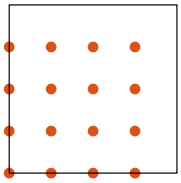

16: (1 6)
-1.7476; 1.792

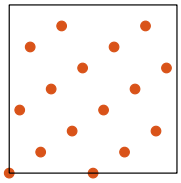

16: (1 3)
-1.669; 4.394

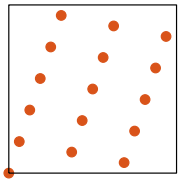

16: (1 7)
-1.5445; 9.114

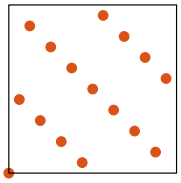

8x2: (1 1), (0 1)
-1.5444; 9.521

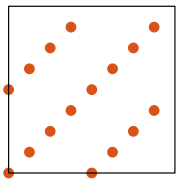

16: (1 2)
-1.0437; 24.25

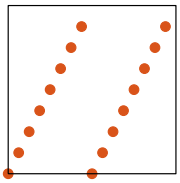

8x2: (1 0), (0 1)
-0.6524; 34.27

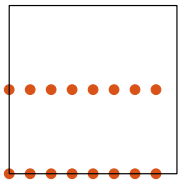

16: (1 8)
-0.6524; 34.27

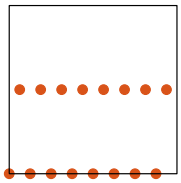

16: (1 1)
1.573; 84.58

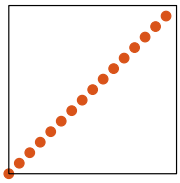

16: (1 0)
6.4651; 185.1

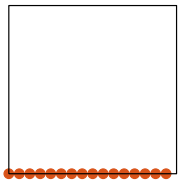

N=17

17: (1 4)
-1.9164; -0.08451

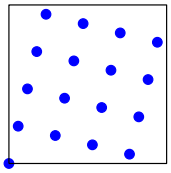

17: (1 5)
-1.8857; 1.034

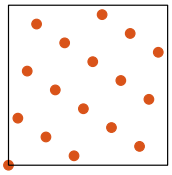

17: (1 3)
-1.7845; 5.946

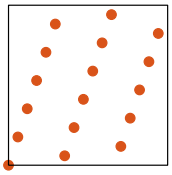

17: (1 2)
-1.0492; 28.24

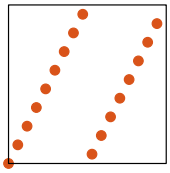

17: (1 1)
1.9435; 96.09

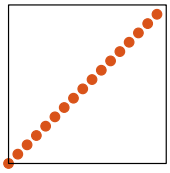

17: (1 0)
7.4954; 209.2

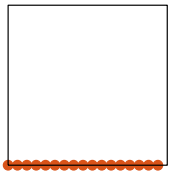

N=18

18: (1 5)
-2.0781; -0.3015

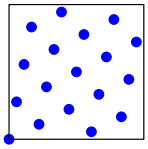

18: (1 4)
-2.0719; 0.5376

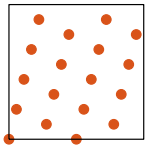

6x3: (1 1), (0 1)
-2.0701; 0.639

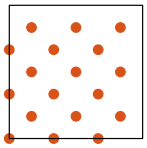

18: (2 3)
-2.0196; 2.98

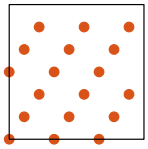

18: (1 3)
-1.8964; 7.245

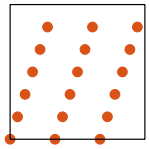

18: (1 6)
-1.8219; 10.37

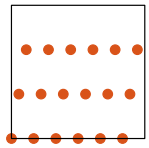

6x3: (1 0), (0 1)
-1.8219; 10.69

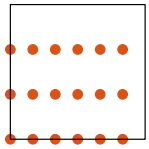

18: (1 8)
-1.7187; 13.63

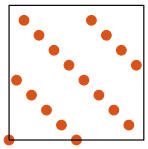

18: (1 2)
-1.0428; 32.89

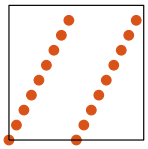

18: (2 9)
-0.52766; 44.84

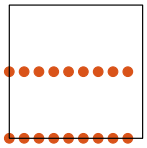

18: (1 9)
-0.52766; 44.83

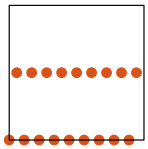

18: (1 1)
2.3509; 109.2

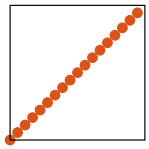

18: (1 0)
8.6045; 236.5

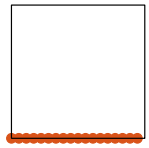

N=19

19: (1 4)
-2.2252; -0.107

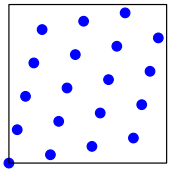

19: (1 7)
-2.1532; 3.773

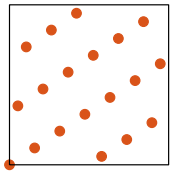

19: (1 3)
-2.0044; 9.386

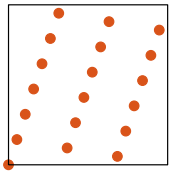

19: (1 2)
-1.0242; 37.55

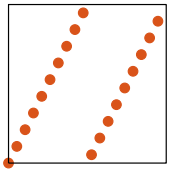

19: (1 1)
2.7956; 122.4

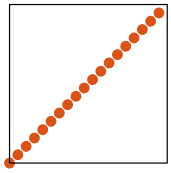

19: (1 0)
9.7924; 263.7

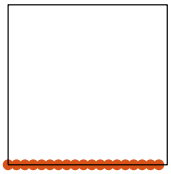

N=20

20: (1 8)
-2.3958; -0.7156

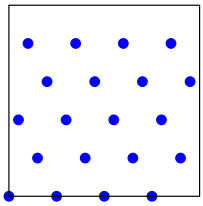

10x2: (1 2), (0 1)
-2.3839; 0.9476

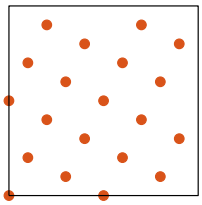

20: (1 4)
-2.3727; 0.9518

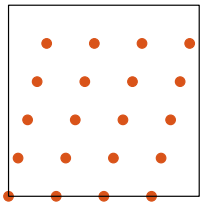

20: (2 5)
-2.3604; 0.9689

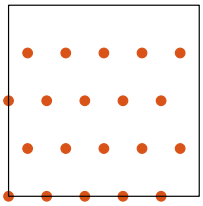

20: (1 5)
-2.3591; 1.7

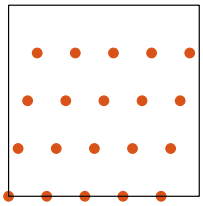

20: (4 5)
-2.3579; 2.429

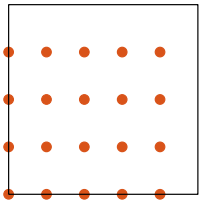

20: (1 6)
-2.284; 5.097

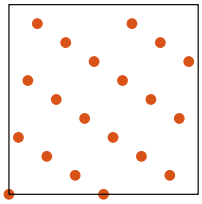

20: (1 3)
-2.1081; 11.88

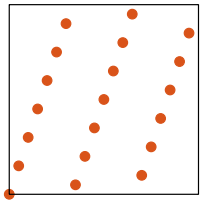

10x2: (1 1), (0 1)
-1.8691; 19.27

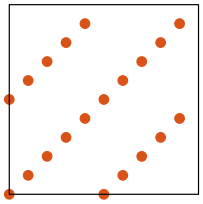

20: (1 9)
-1.869; 19.26

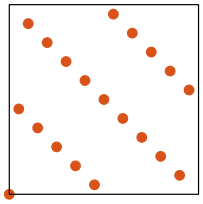

20: (1 2)
-0.99307; 42.84

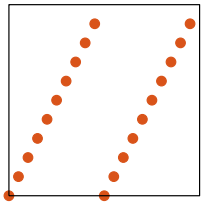

20: (1 10)
-0.33731; 58.54

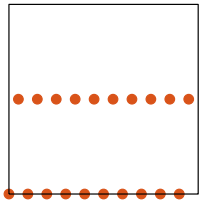

10x2: (1 0), (0 1)
-0.33731; 58.55

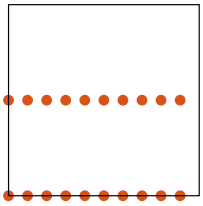

20: (1 1)
3.2778; 137.1

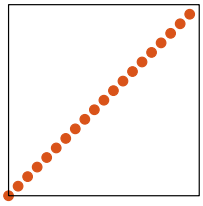

20: (1 0)
11.06; 294.2

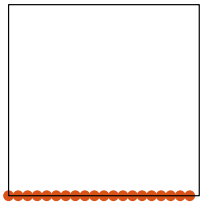

N=21

21: (1 8)
-2.5353; 0.4821

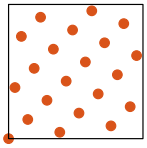

21: (1 6)
-2.532; 1.086

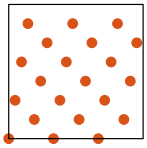

21: (1 4)
-2.5195; 1.43

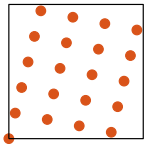

21: (1 9)
-2.4123; 6.087

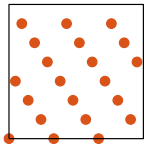

21: (1 3)
-2.2076; 13.76

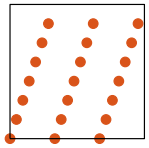

21: (1 7)
-2.0915; 16.93

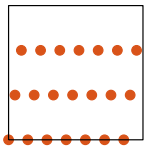

21: (3 7)
-2.0915; 16.99

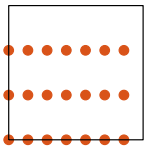

21: (1 2)
-0.94925; 48.12

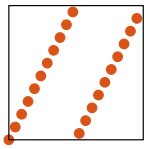

21: (1 1)
3.7976; 151.8

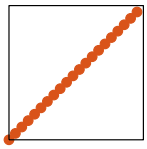

21: (1 0)
12.406; 324.6

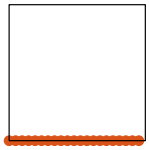

N=22

22: (1 5)
-2.7052; -0.1743

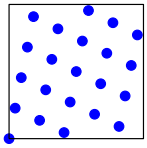

22: (1 6)
-2.703; 0.5395

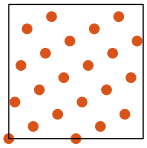

22: (1 4)
-2.6679; 2.498

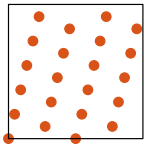

22: (1 8)
-2.5383; 7.413

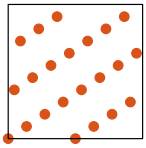

22: (1 3)
-2.3025; 15.93

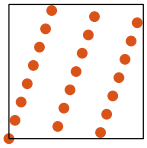

22: (1 10)
-1.9936; 25.14

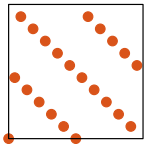

22: (1 2)
-0.89257; 54.03

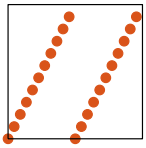

22: (2 11)
-0.079563; 72.25

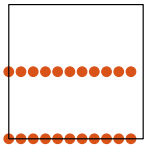

22: (1 11)
-0.079563; 72.25

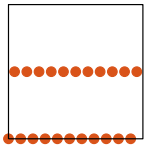

22: (1 1)
4.3554; 168

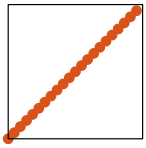

22: (1 0)
13.832; 358.1

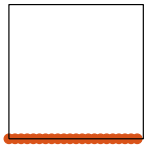

N=23

23: (1 5)
-2.8871; -0.8394

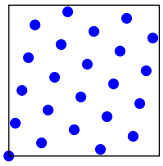

23: (1 4)
-2.8153; 2.436

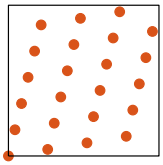

23: (1 7)
-2.6612; 9.195

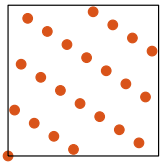

23: (1 3)
-2.3927; 18.34

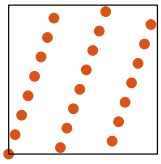

23: (1 2)
-0.82283; 59.95

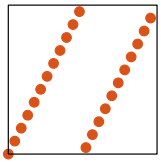

23: (1 1)
4.9511; 184.3

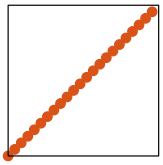

23: (1 0)
15.338; 391.7

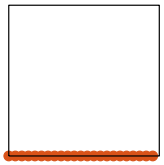

N=24

24: (1 5)
-3.0511; -0.3301

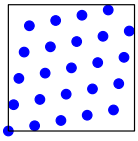

24: (3 4)
-3.0447; -0.06704

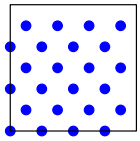

12x2: (1 2), (0 1)
-3.0177; 0.5999

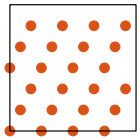

24: (1 10)
-3.0144; 2.317

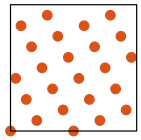

24: (1 9)
-2.9838; 2.006

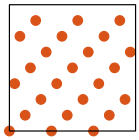

24: (1 7)
-2.9825; 4.138

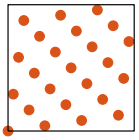

24: (1 4)
-2.9598; 3.91

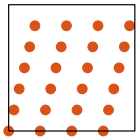

12x2: (1 3), (0 1)
-2.9295; 4.419

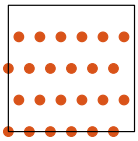

24: (1 6)
-2.9292; 5.318

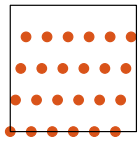

12x2: (2 3), (1 0)
-2.9289; 6.289

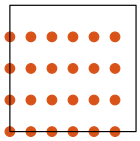

24: (2 3)
-2.7813; 10.92

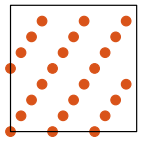

24: (1 3)
-2.478; 21.08

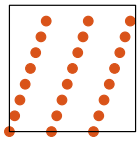

24: (1 8)
-2.3119; 26.29

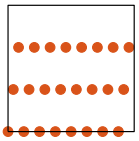

24: (3 8)
-2.3119; 26.36

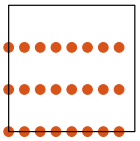

24: (1 11)
-2.0911; 32.55

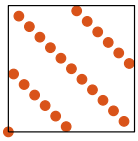

12x2: (1 1), (0 1)
-2.0911; 32.59

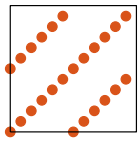

24: (1 2)
-0.73989; 66.48

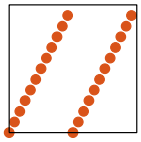

12x2: (1 0), (0 1)
0.24702; 89.1

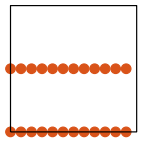

24: (1 12)
0.24702; 89.1

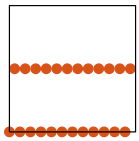

24: (1 1)
5.5851; 202.2

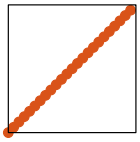

24: (1 0)
16.923; 428.4

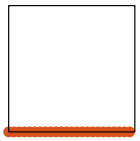

N=25

25: (1 10)
-3.2153; -0.2049

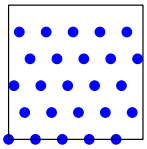

25: (1 5)
-3.207; 0.3679

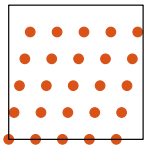

5x5: (1 0), (0 1)
-3.2019; 1.069

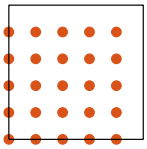

25: (1 7)
-3.2019; 0.4053

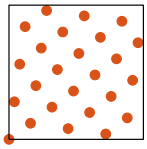

25: (1 4)
-3.1025; 5.31

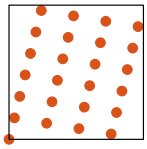

25: (1 9)
-2.8983; 12.67

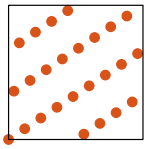

25: (1 3)
-2.5583; 23.98

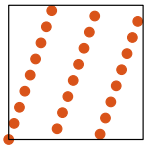

25: (1 2)
-0.6436; 73.02

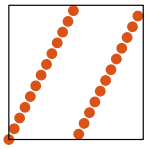

25: (1 1)
6.2575; 220

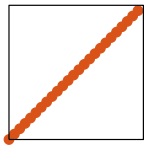

25: (1 0)
18.589; 465.1

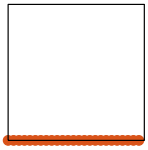

N=26

26: (1 10)
-3.3767; 0.2446

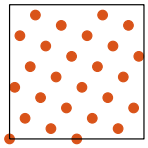

26: (1 5)
-3.3705; 0.08597

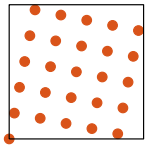

26: (1 6)
-3.3256; 2.229

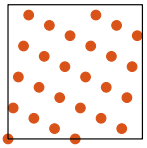

26: (1 7)
-3.3237; 3.434

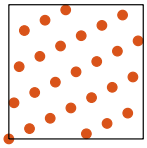

26: (1 4)
-3.2441; 7.145

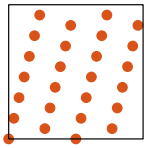

26: (1 8)
-3.012; 15.45

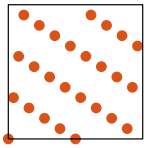

26: (1 3)
-2.6334; 27.19

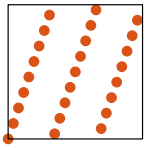

26: (1 12)
-2.1601; 39.99

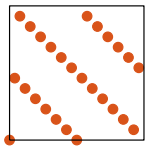

26: (1 2)
-0.53382; 80.19

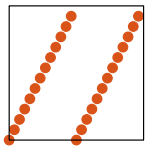

26: (1 13)
0.64367; 105.9

26: (2 13)
0.64367; 105.9

26: (1 1)
6.9683; 239.4

26: (1 0)
20.335; 504.9

N=27

27: (1 6)
-3.5459; -0.02064

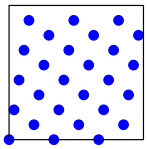

27: (1 5)
-3.5438; 0.4978

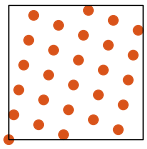

9x3: (1 1), (0 1)
-3.4222; 5.454

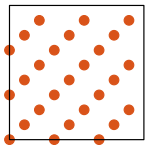

27: (1 8)
-3.4217; 6.523

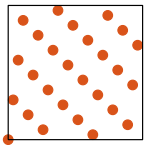

27: (1 4)
-3.3841; 7.452

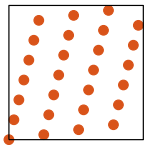

27: (1 12)
-3.1224; 17.14

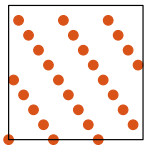

27: (1 3)
-2.7033; 30.23

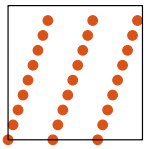

27: (1 9)
-2.479; 35.87

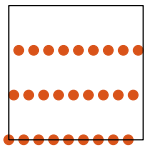

9x3: (1 0), (0 1)
-2.479; 35.89

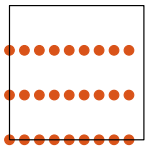

27: (1 2)
-0.41044; 87.35

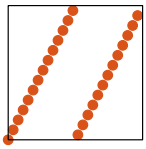

27: (1 1)
7.7177; 258.9

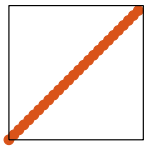

27: (1 0)
22.161; 544.8

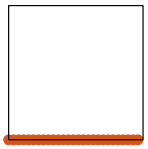

N=28

28: (1 6)
-3.7307; -0.8483

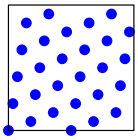

28: (1 5)
-3.7174; -0.188

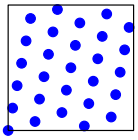

28: (1 8)
-3.7049; 1.889

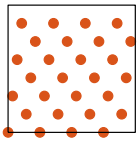

28: (1 12)
-3.6291; 4.103

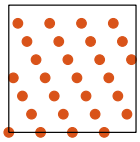

14x2: (1 2), (0 1)
-3.6287; 5.31

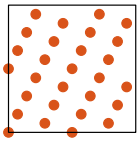

28: (1 4)
-3.5218; 8.495

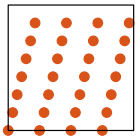

28: (2 7)
-3.4692; 10.58

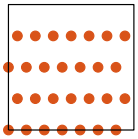

28: (1 7)
-3.4692; 10.9

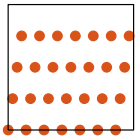

28: (4 7)
-3.4691; 11.21

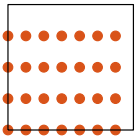

28: (1 10)
-3.2293; 19.47

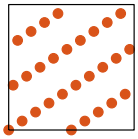

28: (1 3)
-2.7678; 33.58

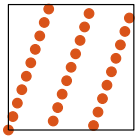

14x2: (1 1), (0 1)
-2.1997; 48.97

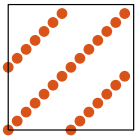

28: (1 13)
-2.1997; 48.96

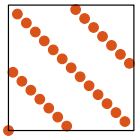

28: (1 2)
-0.27334; 95.14

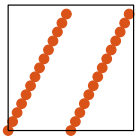

14x2: (1 0), (0 1)
1.1114; 125.9

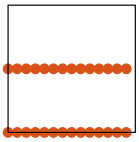

28: (1 14)
1.1114; 125.9

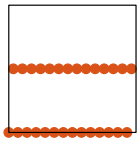

28: (1 1)
8.5058; 279.8

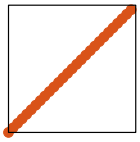

28: (1 0)
24.067; 587.8

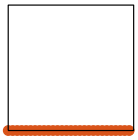

N=29

29: (1 12)
-3.8854; 1.049

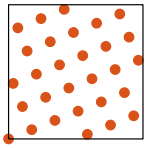

29: (1 5)
-3.8843; 0.115

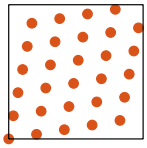

29: (1 8)
-3.8697; 1.923

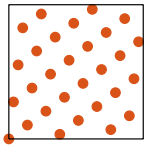

29: (1 4)
-3.6574; 10.55

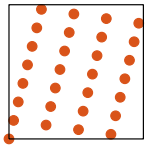

29: (1 9)
-3.3327; 21.66

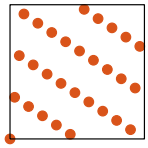

29: (1 3)
-2.8268; 36.96

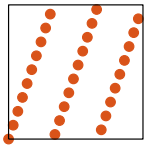

29: (1 2)
-0.12242; 103

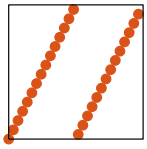

29: (1 1)
9.3328; 300.8

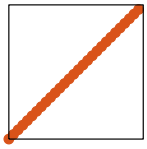

29: (1 0)
26.054; 630.7

N=30

30: (3 5)
-4.0847; -0.8149

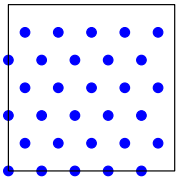

30: (2 5)
-4.0723; -0.4116

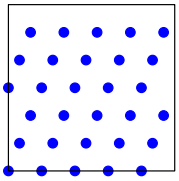

30: (1 5)
-4.0469; 1.91

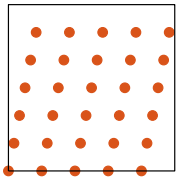

30: (1 12)
-4.0385; 1.172

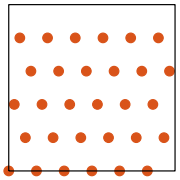

30: (2 9)
-4.0385; 1.13

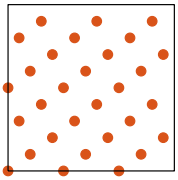

30: (1 6)
-4.0357; 2.028

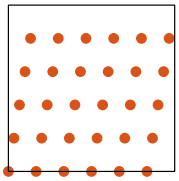

30: (5 6)
-4.0339; 3.382

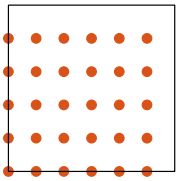

30: (1 7)
-3.9282; 5.804

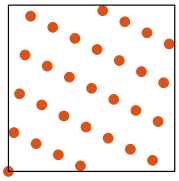

30: (1 8)
-3.9274; 7.259

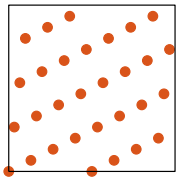

30: (1 9)
-3.8453; 10.15

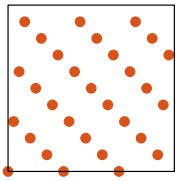

30: (1 11)
-3.8451; 10.08

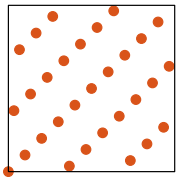

30: (1 4)
-3.7909; 12.3

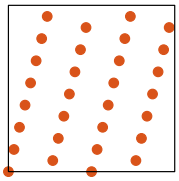

30: (2 3)
-3.4324; 24.42

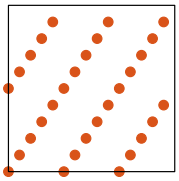

30: (1 3)
-2.8802; 40.63

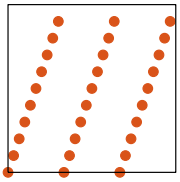

30: (1 10)
-2.5893; 48.55

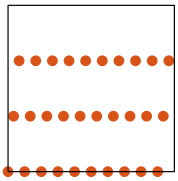

30: (3 10)
-2.5893; 48.55

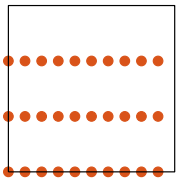

30: (1 14)
-2.2091; 57.97

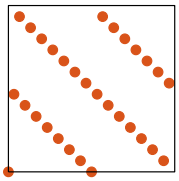

30: (1 2)
0.042423; 111.4

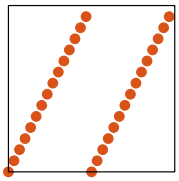

30: (2 15)
1.6511; 145.9

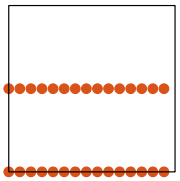

30: (1 15)
1.6511; 145.9

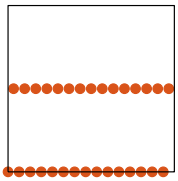

30: (1 1)
10.199; 323.4

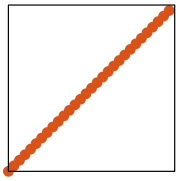

30: (1 0)
28.121; 676.9

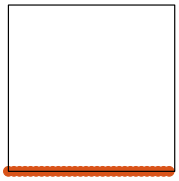

Appendix C: Stability of lattices as a function of aspect ratio

The effect of aspect ratio on stability of various lattices is illustrated in figures below. For N as indicated, the left figure enumerates all non-equivalent lattices for a rectangle. These are superset of non-equivalent lattices on a square. For example for $N = 8$, lattices number 5 and 6 are equivalent for a square but not equivalent for a rectangle (the total number of non-equivalent lattices on a rectangle is given by sequence https://oeis.org/A069734 in OEIS). Figure on the right shows the stability of each of the lattices as a function of aspect ratio L/H. Without loss of generality (by interchanging L and H) we took the aspect ratio to be between 0 and 1. Black squares indicate stable regime, white unstable regime.

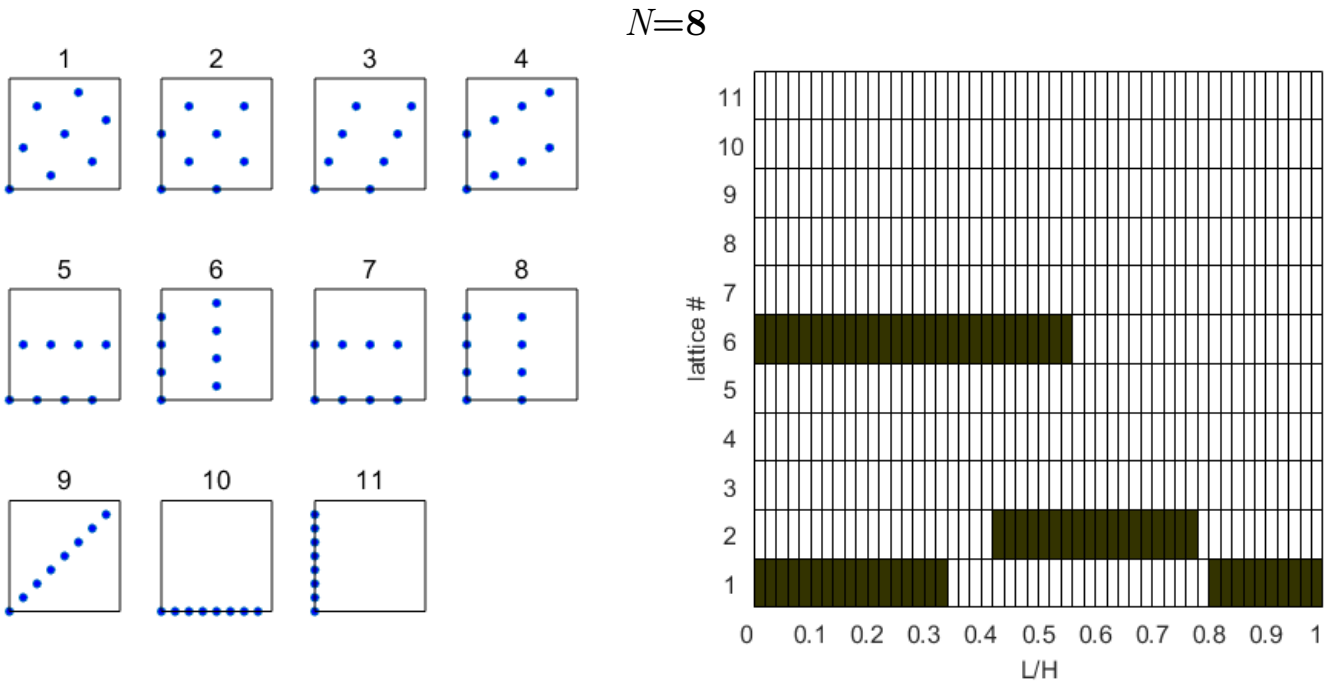

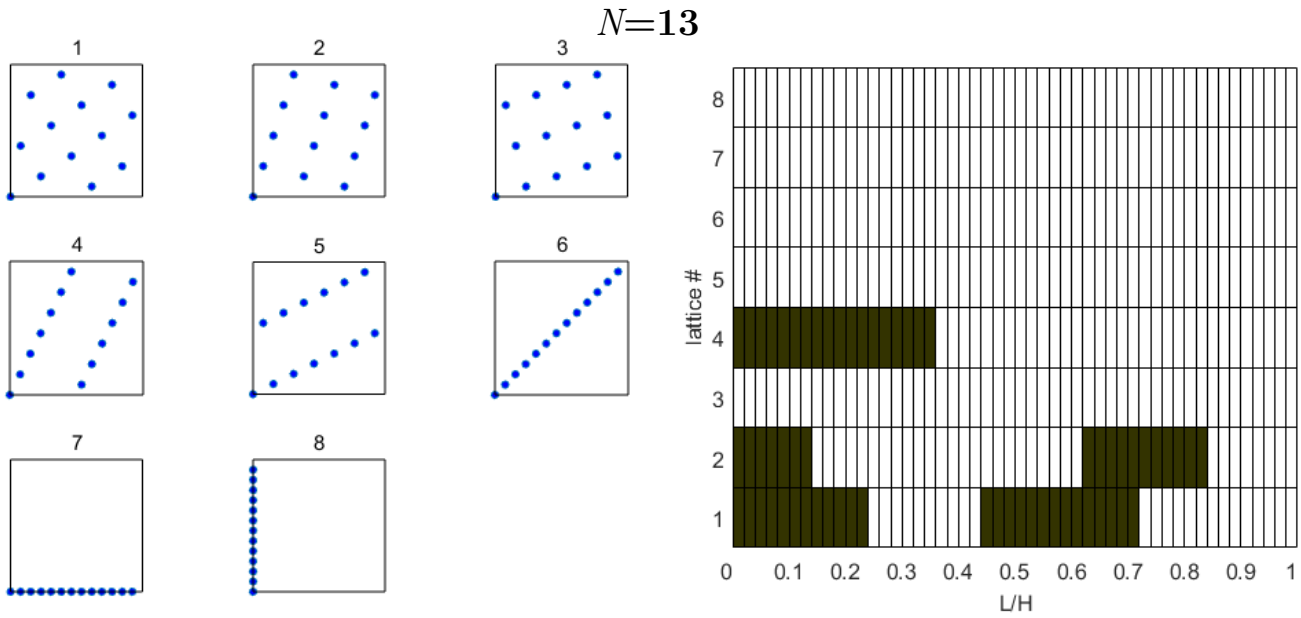

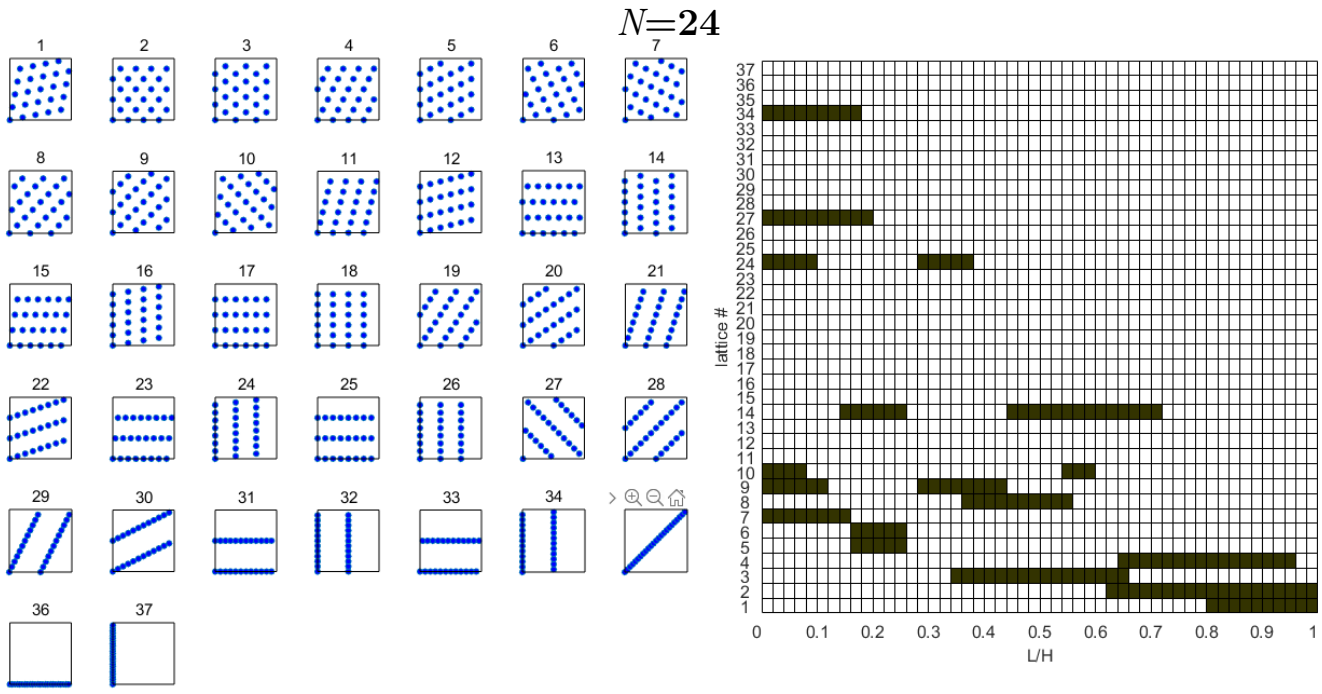

[1] T. Kolokolnikov, M. Ward, A ring of spikes in a schnakenberg model, Physica D: Nonlinear Phenomena 441 (2022) 133521.

[2] T. Kolokolnikov, J. Wei, Hexagonal spike clusters for some pde's in 2d, Discrete and Continuous Dynamical Systems-B 25 (10) (2020) 4057–4070.

[3] A. Turing, The chemical basis of morphogenesis, Phil Trans R Soc B 237 (1952) 37–72.

[4] A. Cheviakov, M. Ward, Optimization of trap locations for narrow capture problems, in: Target Search Problems, Springer, 2024, pp. 225–246.

[5] A. F. Cheviakov, M. J. Ward, Optimizing the principal eigenvalue of the laplacian in a sphere with interior traps, Mathematical and Computer Modelling 53 (7-8) (2011) 1394–1409.

[6] P. C. Bressloff, S. D. Lawley, Stochastically gated diffusion-limited reactions for a small target in a bounded domain, Physical Review E 92 (6) (2015) 062117.

[7] T. Kolokolnikov, M. S. Titcombe, M. J. Ward, Optimizing the fundamental neumann eigenvalue for the laplacian in a domain with small traps, European Journal of Applied Mathematics 16 (2) (2005) 161–200.

[8] S. Redner, A guide to first-passage processes, Cambridge university press, 2001.

[9] A. Singer, Z. Schuss, D. Holcman, Narrow escape, part ii: The circular disk, Journal of statistical physics 122 (3) (2006) 465–489.

[10] S. A. Iyaniwura, T. Wong, C. B. Macdonald, M. J. Ward, Optimization of the mean first passage time in near-disk and elliptical domains in 2-d with small absorbing traps, SIAM Review 63 (3) (2021) 525–555.

[11] J. Wei, M. Winter, Stationary multiple spots for reaction–diffusion systems, Journal of mathematical biology 57 (1) (2008) 53–89.

[12] T. Wong, M. J. Ward, Spot patterns in the 2-d schnakenberg model with localized heterogeneities, arXiv preprint arXiv:2009.07882 (2020).

[13] M. J. Ward, D. McInerney, P. Houston, D. Gavaghan, P. Maini, The dynamics and pinning of a spike for a reaction-diffusion system, SIAM Journal on Applied Mathematics 62 (4) (2002) 1297–1328.

[14] T. Kolokolnikov, M. J. Ward, Reduced wave green's functions and their effect on the dynamics of a spike for the gierer-meinhardt model, European Journal of Applied Mathematics 14 (5) (2003) 513–546.

[15] A. Hanany, D. Orlando, S. Reffert, Sublattice counting and orbifolds, Journal of High Energy Physics 2010 (6) (2010) 1–24.

[16] Source code and movies available from the authors, see `http://www.mathstat.dal.ca/~tkolokol/periodic`.

[17] T. Kolokolnikov, M. J. Ward, J. Wei, Spot self-replication and dynamics for the schnakenburg model in a two-dimensional domain, Journal of nonlinear science 19 (1) (2009) 1–56.

[18] T. Kolokolnikov, F. Paquin-Lefebvre, M. J. Ward, Competition instabilities of spike patterns for the 1d gierer–meinhardt and schnakenberg models are subcritical, Nonlinearity 34 (1) (2021) 273.